

1986

# A study of the early voltage and common-emitter current gain in complementary bipolar transistors /

Stephen E. Parks  
*Lehigh University*

Follow this and additional works at: <https://preserve.lehigh.edu/etd>



Part of the [Electrical and Computer Engineering Commons](#)

---

## Recommended Citation

Parks, Stephen E., "A study of the early voltage and common-emitter current gain in complementary bipolar transistors /" (1986).  
*Theses and Dissertations*. 4646.  
<https://preserve.lehigh.edu/etd/4646>

This Thesis is brought to you for free and open access by Lehigh Preserve. It has been accepted for inclusion in Theses and Dissertations by an authorized administrator of Lehigh Preserve. For more information, please contact [preserve@lehigh.edu](mailto:preserve@lehigh.edu).

A STUDY OF THE  
EARLY VOLTAGE AND COMMON-EMITTER CURRENT GAIN  
IN COMPLEMENTARY BIPOLAR TRANSISTORS

by

Stephen E. Parks

A Thesis

Presented to the Graduate Committee

of Lehigh University

in Candidacy for the Degree of

Master of Science

in

Electrical Engineering

1986

CERTIFICATE OF APPROVAL

This thesis is accepted and approved in partial fulfillment of the requirements for the degree of Master of Science in the Department of Computer Science and Electrical Engineering.

May 15, 1986  
Date

Frank H. Hielscher  
Professor in Charge

Erin D. Thompson  
Chairman of Department

## ACKNOWLEDGEMENTS

I wish to acknowledge the support and guidance of my advisor, Dr. Frank H. Hielscher, and I would like to thank the following employees at AT&T Bell Laboratories for their help throughout my thesis: Mr. Wallace H. Eckton Jr., Mr. Kem K. Ferridun, Mr. James R. Mathews, Mr. Stanley F. Moyer, and Mr. Harvey D. Seidel. Also, I would like to thank Margaret Napaletano, Glen Johnson, and Leora Gilfert for their work in obtaining the necessary electrical measurements. Finally, I wish to thank Mr. William A. Griffin and Mr. Eugene G. Parks at AT&T Technology Systems for encouraging the completion of this study.

## TABLE OF CONTENTS

	<u>Page</u>
TITLE	i
CERTIFICATE OF APPROVAL	ii
ACKNOWLEDGEMENTS	iii
TABLE OF CONTENTS	iv
LIST OF TABLES	v
LIST OF FIGURES	vi
ABSTRACT	1
I. INTRODUCTION	3
II. THEORETICAL BACKGROUND	6
Early Effect	6
Derivation of Early Voltage	10
Common-Emitter Current Gain	17
III. EXPERIMENTAL BACKGROUND	30
Overview of Complementary Bipolar Processing Technology	30
Electrical Measurements of Complementary Bipolar Transistors	32
Discussion of Diffusion Profile Measurement Techniques	36
IV. EXPERIMENTAL RESULTS	42
V. DISCUSSION OF RESULTS	51
VI. CONCLUSION	60
REFERENCES	64
VITA	68

## LIST OF TABLES

	<u>Page</u>
Table I - Electrical measurements of $I_S$ , $V_A$ , and $\beta$ for the CBIC npn and pnp transistors	32
Table II - Metallurgical junction depths, zero-bias depletion region, and electrical base widths obtained from a numerical solution of Poisson's equation for CBIC npn and pnp doping profiles	42
Table III - Electrical measurements and theoretically calculated values of van der Pauw (VDP) sheet resistances for CBIC npn and pnp doping profiles	45
Table IV - Theoretically calculated device parameters for the CBIC npn and pnp transistors used in calculations of $I_S$ , $V_A$ , and $\beta$	49
Table V - Comparison of electrical measurements and theoretically calculated values of $I_S$ , $V_A$ , and $\beta$ for the CBIC npn and pnp transistors	50

## LIST OF FIGURES

	<u>Page</u>
Figure 1 - Bipolar transistor output characteristics showing the Early voltage, $V_A$	7
Figure 2 - A typical npn bipolar transistor in a common-emitter configuration biased in the forward active region	8
Figure 3 - a. Net impurity concentration for a vertical pnp transistor - after Malone <sup>7</sup> b. Vertical pnp Early voltage $V_A$ versus $\beta$ for 8 ohm-cm collector resistivity - after Malone <sup>7</sup>	13 13
Figure 4 - A theoretically calculated effective emitter profile $N_{eff}(x)$ showing the difference in $Q_E$ and $Q_{Eeff}$ due to bandgap narrowing in the heavily doped emitter	21
Figure 5 - Electrical $\Delta E_g^{el}$ and optical $\Delta E_g^{op}$ bandgap narrowing measurements versus doping concentration in highly doped n-type silicon - after Lee and Fossum <sup>26</sup>	28
Figure 6 - Majority and minority hole mobilities versus concentration N	29
Figure 7 - CBIC device structure	31
Figure 8 - Electrical measurements of $I_C$ versus $V_{CE}$ for CBIC npn and pnp transistors	33
Figure 9 - Electrical measurements of $\beta$ versus $I_C$ for CBIC npn and pnp transistors	34
Figure 10 - Electrical measurements of $I_C$ and $I_B$ vs. $V_{BE}$ for CBIC npn and pnp transistors	35
Figure 11 - A bevelled sample of an npn transistor prepared for spreading resistance measurements	37
Figure 12 - Determination of junction depth XJ using angle-lap and stain measurements	39
Figure 13 - A van der Pauw (VDP) sheet resistor suitable for characterizing impurity layers. The outer four pads are used for probing the structure.	41

	<u>Page</u>
Figure 14 - CBIC npn transistor - spreading resistance and SUPREM simulation profiles	43
Figure 15 - CBIC pnp transistor - spreading resistance and SUPREM simulation profiles	44
Figure 16 - Electrical base width $W_B$ vs. collector-to-base voltage $V_{CB}$ for CBIC npn and pnp profiles obtained from a numerical solution of Poisson's equation	47
Figure 17 - $\partial W_B / \partial V_{CB}$ vs. $V_{CB}$ for CBIC npn and pnp transistors	56
Figure 18 - Electrical measurements of $1/f_T$ vs. $1/I_C$ for CBIC npn and pnp transistors	58



## ABSTRACT

The Complementary Bipolar Integrated Circuit (CBIC) process results in both high performance vertical npn and vertical pnp transistors on the same silicon chip. While the common-emitter current gains are nearly identical, however, the corresponding Early voltages are significantly different. The Early voltage of the npn transistor is typically three times higher than the pnp transistor for the same value of common-emitter current gain. This study provides a theoretical basis for the Early voltage difference in complementary npn and pnp transistors.

The Early voltage is strongly dependent on the Gummel number in the base and the doping profiles of the base and collector regions. A higher Gummel number and a slower rate of change in the decrease of the electrical base width as a function of collector-to-base reverse bias, both result in an increase in the Early voltage. The common-emitter current gain is a function of the base transport factor and the emitter efficiency. For modern planar bipolar transistors, the base transport factor is essentially unity and the emitter efficiency limits the value of the common-emitter current gain. A reduction in the emitter efficiency is primarily due to bandgap narrowing in the heavily doped emitter. But, electric field effects and an increase in Auger recombination also serve to degrade the emitter efficiency.

The theoretical calculations of Early voltage and common-emitter current gain were obtained using spreading resistance measurements and SUPREM process simulations to determine the electrically active dopant profiles. No assumptions were made concerning the shape and magnitude of the doping profiles. A numerical

solution of Poisson's equation was used to find a mathematical relationship between the electrical base width and the collector-to-base reverse bias. The zero-bias depletion region widths were also obtained from a numerical analysis, and they were included in the values calculated for the electrical base widths. The common-emitter current gain was evaluated from an emitter efficiency limited expression taking into account bandgap narrowing effects. The theoretical values of Early voltage and common-emitter current gain are shown to agree reasonably well with the electrical measurements.

## I. INTRODUCTION

The influence of space-charge layer widening in bipolar junction transistors was first described by J. M. Early in 1952.<sup>1</sup> He noted that the base width  $W_B$  of a transistor decreased as the collector-to-base voltage  $V_{CB}$  increased resulting in two principal effects. First, a decrease in  $W_B$  would decrease the recombination of injected minority carriers in the base since the carriers would diffuse across the base in a shorter time and, therefore, increase the base transport factor  $\alpha_T$ . Second, a decrease in  $W_B$  would decrease the impedance presented to the minority carrier current injected by the emitter by increasing the carrier gradient and, therefore, increase the emitter efficiency  $\gamma$ . Both of these effects would result in an increase in the common-base current gain  $\alpha_F$  since  $\alpha_F \equiv \alpha_T \gamma$ .

Early's discovery necessitated changes in the Ebers-Moll model<sup>2</sup> which was widely used to simulate static behavior of bipolar transistor circuits. Lindholm and Hamilton<sup>3</sup> in 1971, and later Jaeger and Brodersen<sup>4</sup> in 1978, showed that through the addition of a single parameter, called the Early voltage  $V_A$ , the Early effect could be incorporated into the Ebers-Moll formulation. The Early voltage would take into account the nonzero slope in the collector current  $I_C$  versus collector-to-emitter voltage  $V_{CE}$  curves.

The common-emitter current gain  $\beta$  is related to the common-base current gain  $\alpha_F$  by  $\beta = \alpha_F / (1 - \alpha_F)$ . For modern planar bipolar transistors, operating at intermediate current levels,  $\alpha_T$  is essentially unity and  $\beta$  is limited by the emitter efficiency  $\gamma$ . To achieve high transistor  $\beta$ 's (100 - 200), the emitter is much more heavily doped than the base. Theoretical calculations of  $\beta$  are several orders of

4

magnitude higher than measured, however, since the effective emitter doping profile is lower than the actual emitter doping profile. As the emitter doping becomes very high, several heavy doping effects cause a reduction in the actual emitter doping profile, and, therefore, the calculated value of emitter efficiency. They include: 1.) bandgap narrowing, 2.) a changing electric field, and 3.) Auger recombination.<sup>44</sup>

Although the Early voltage and common-emitter current gain are of little importance in digital circuits, in linear (analog) circuits they do play a significant role in circuit performance. The Early voltage mismatch between emitter-coupled pair transistors limits the attainable common-mode rejection ratio CMRR and power supply rejection ratio PSRR of a simple resistively loaded bipolar differential amplifier.<sup>5</sup> The incremental output resistance of different current sources (for example, a Wilson current mirror) is directly proportional to the Early voltage of the output transistor.<sup>6</sup> Indeed, if two transistors are required to carry the same amount of current and if they have significantly different collector-to-emitter voltages, the Early voltage should be high to achieve reasonable current matching. The common-emitter current gain ( $\beta = \Delta I_C / \Delta I_B$ ) is an important measure of how well a transistor will amplify an input signal when biased in the forward active region. If the transistor is meant to amplify effectively, the base current should be appreciably smaller than the collector current.

Because of the importance of Early voltage and common-emitter current gain in linear circuit design, the influence of processing parameters on  $V_A$  and  $\beta$  should be studied. In 1977, Malone<sup>7</sup> calculated and compared experimental findings of  $V_A$  and  $\beta$  with theory for a vertical pnp transistor. In 1978, Malhi and Salama<sup>8</sup> did a

similar investigation as Malone, but for a lateral pnp transistor. In both cases, however, they assumed that the common-emitter current gain was base transport limited and that the doping profiles in the base and collector regions were either linearly graded or constant.

The purpose of this work was to investigate the  $V_A - \beta$  relationship in both vertical npn and vertical pnp transistors fabricated together in a complementary bipolar processing technology. Spreading resistance and a SUPREM process simulation, angle-lap and stain, and van der Pauw measurements were used to obtain the electrically active dopant profiles, metallurgical junction depths, and sheet resistances (no assumptions were made about the doping profiles). The common-emitter current gain was evaluated from an emitter efficiency limited expression, taking into account bandgap narrowing in the heavily doped emitter. To obtain a theoretical value of Early voltage, a numerical solution of Poisson's equation was required to quantify the narrowing of the electrical base width as a function of an applied collector-to-base reverse bias.

Before presenting the results of this investigation, a detailed explanation of the Early effect and common-emitter current gain will be reviewed. Also, an overview of the complementary bipolar integrated circuit process technology, electrical measurements of complementary npn and pnp bipolar transistors, and a discussion of the diffusion profile measurement techniques will be included.

## II. THEORETICAL BACKGROUND

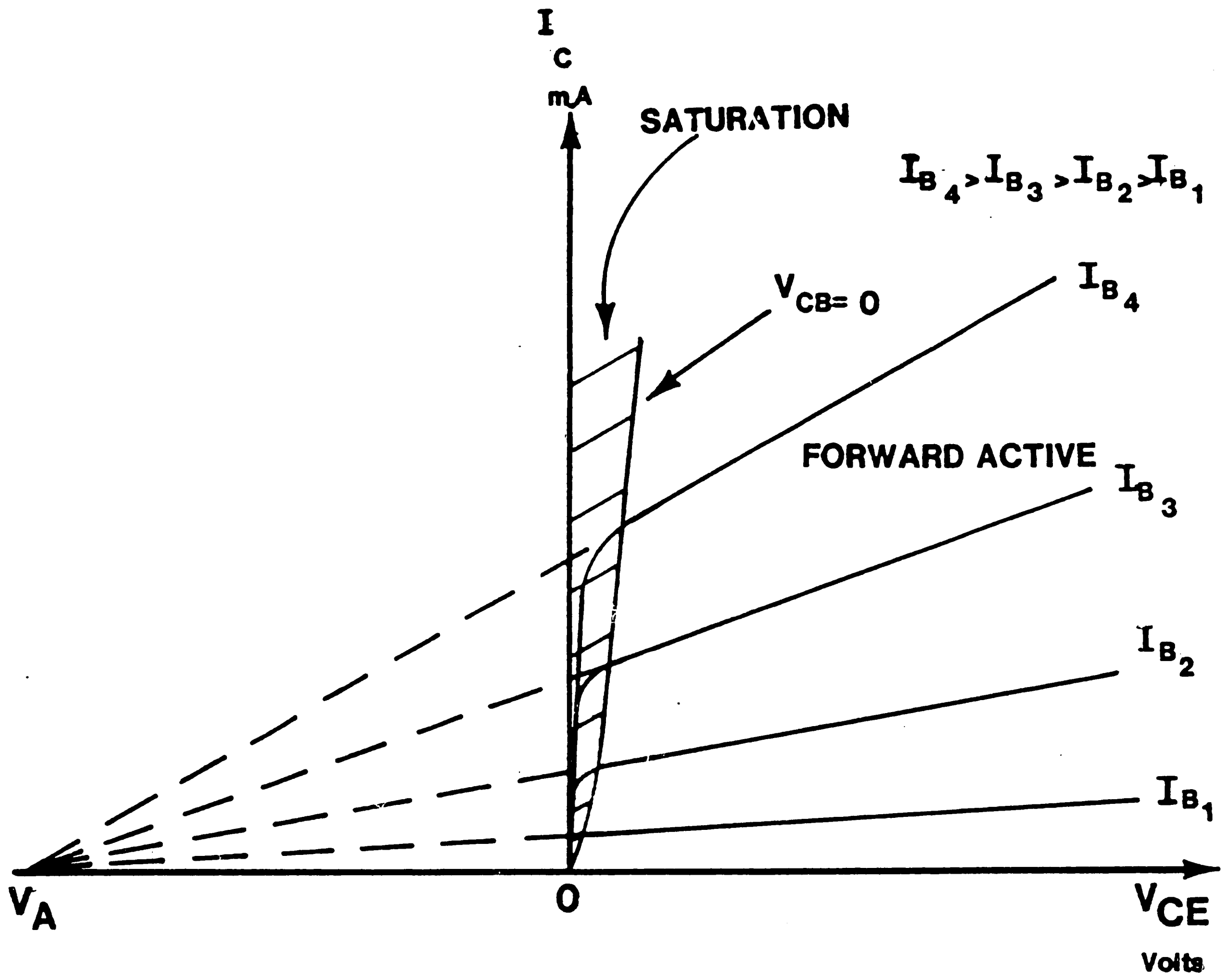
### Early Effect

By definition, the Early voltage  $V_A$  is the intercept on the collector-to-emitter voltage  $V_{CE}$  axis from the projection in the forward active region of the collector current  $I_C$  versus  $V_{CE}$  curves to zero collector current (see Figure 1). The existence of a finite slope in the curves indicates that an increasing  $V_{CE}$  causes an increase in  $I_C$  for a given level of base current  $I_B$ . As Early<sup>1</sup> showed, an increase in the collector-to-base voltage  $V_{CB}$  causes a decrease in the base width  $W_B$  of a transistor. The decrease in  $W_B$  then causes an increase in  $I_C$ . This concept is commonly referred to as the base width modulation or Early effect.

For an npn (pnp) transistor in the forward active region, the collector current is the result of minority carrier electrons (holes) in the base diffusing in the direction of the concentration gradient and being swept across the collector-base depletion region by the electric field  $\mathcal{E}_{CB}$ . The minority carrier electrons (holes) are injected from the emitter, which is forward biased with respect to the base. As  $V_{CE}$  increases the collector-base junction becomes more reversed biased and the collector-base depletion region width  $W_{DCB}$  must increase to sustain the higher voltage. If we assume the forward biased base-to-emitter voltage  $V_{BE}$  remains constant (typically  $\approx 0.75$  V), then the emitter-base depletion width  $W_{DEB}$  also remains constant, and a decrease in  $W_B$  is directly a result of an increase in  $W_{DCB}$ . Since

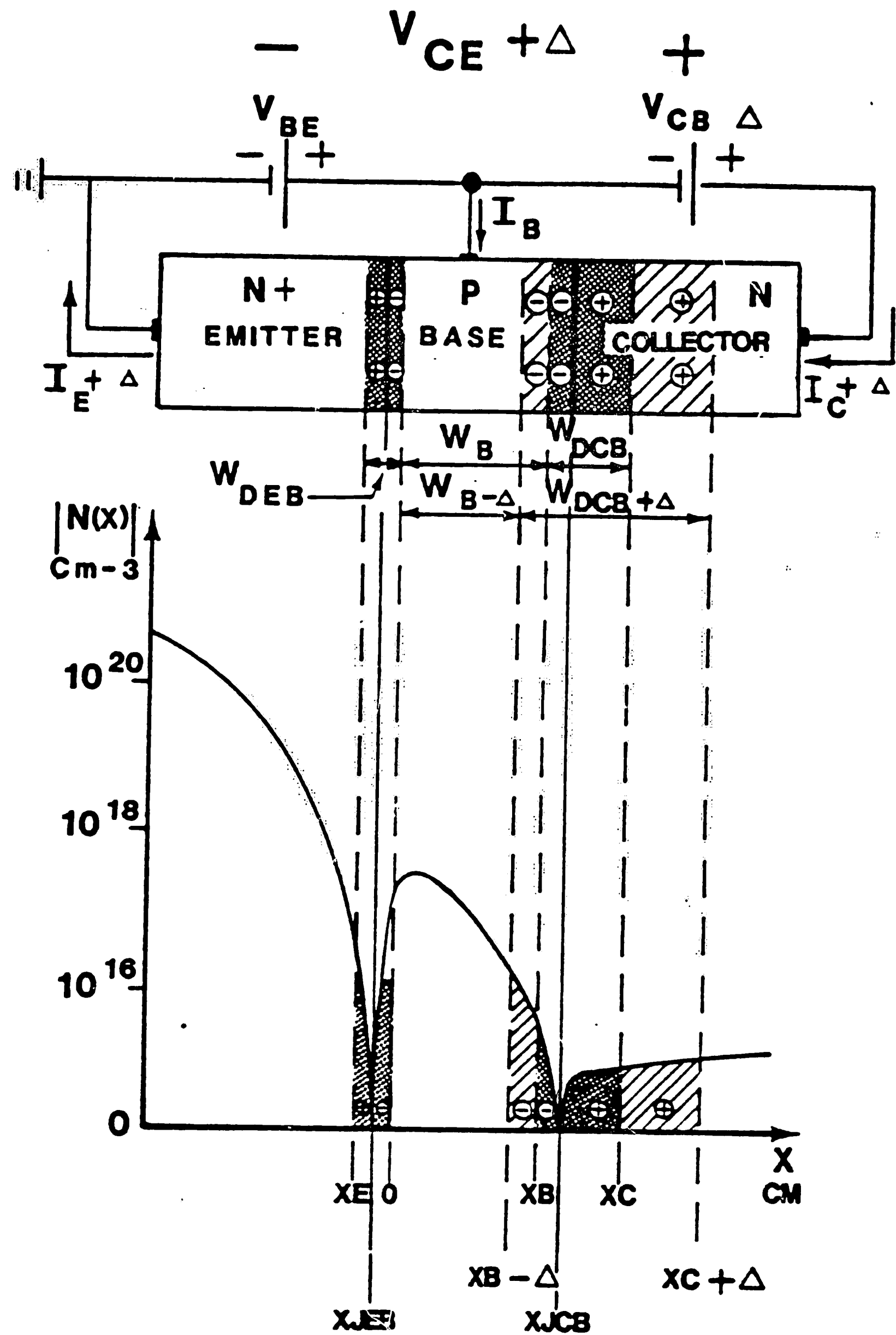
$$V_{CE} = V_{CB} + V_{BE} \quad (1)$$



the increase in  $W_{DCB}$  is obviously due to the reverse bias  $V_{CB}$  on the collector-base junction (see Figure 2).



Bipolar transistor output characteristics showing  
the Early voltage,  $V_A$

Figure 1



$+\Delta$  increase     Initial depletion region     $\oplus$  uncompensated positive donor ions  
 $-\Delta$  decrease     extended depletion region due to increase in  $V_{CE}$      $\ominus$  uncompensated negative acceptor ions

A typical npn bipolar transistor in a common-emitter configuration biased in the forward active region

Figure 2



The dependence of  $V_{CB}$  on the electric field  $\mathcal{E}_{CB}$  and the depletion region width  $W_{DCB}$  is a direct result of Poisson's equation<sup>9</sup>:

$$\partial^2 \Phi / \partial x^2 = - \partial \mathcal{E} / \partial x = -\rho / \epsilon_s \quad (2)$$

where  $\Phi$  is the potential difference in the depletion region equal to

$$\Phi = V_{CB} + \Phi_{iCB} \text{ (built-in potential of collector-base junction)} \quad (3)$$

$\mathcal{E}$  is the electric field in the depletion region equal to  $\mathcal{E}_{CB}$ ,  $\rho$  is the space-charge density equal to

$$\rho = q (p(x) - n(x) + N_D(x) - N_A(x)) \quad (4)$$

$p(x)$  = mobile hole carrier concentration density

$n(x)$  = mobile electron carrier concentration density

$N_D(x)$  = ionized donor concentration density

$N_A(x)$  = ionized acceptor concentration density

$q$  is the electron charge, and  $\epsilon_s$  is the permittivity of the silicon ( $1.04 \times 10^{-12}$  F/cm).

Assuming the net carrier concentration  $p(x) - n(x)$  is much less than the net ionized dopant density  $N_D(x) - N_A(x)$  in the depletion region, by combining equations (2), (3), and (4) we can write

$$\partial^2 (V_{CB} + \Phi_{iCB}) / \partial x^2 = - \partial \mathcal{E}_{CB} / \partial x = -q (N_D(x) - N_A(x)) / \epsilon_s \quad (5)$$

If we define

$$N(x) = |N_D(x) - N_A(x)| \quad (6)$$

a single integration of equation (5) results in

$$\mathcal{E}_{CB} = -q / \epsilon_s \left( \int_{x_B}^{x_C} N(x) \partial x \right) \quad (7)$$

and a double integration of equation (5) results in

$$V_{CB} = \int_{x_B}^{x_C} \left( \int_x^{x_C} N(x) \partial x \right) \partial x \quad (8)$$

where  $X_B$  and  $X_C$  are the boundaries of the collector-base depletion region in the base and the collector respectively.

Equation (8) can be expanded to

$$V_{CB} = -q/\epsilon_s \left[ \int_{X_B}^{X_C} \left( \int_x^{X_{JCB}} N(x) dx + \int_{X_{JCB}}^{X_C} N(x) dx \right) dx \right] - \Phi_{iCB} \quad (9)$$

where  $X_{JCB}$  is the metallurgical collector-base junction depth, and

$$\int_{X_B}^{X_{JCB}} N(x) dx = \int_{X_{JCB}}^{X_C} N(x) dx \quad (10)$$

to maintain overall space charge neutrality. Equation (9) is not an easy equation to solve in closed form, and the solution usually requires a numerical technique done by a computer. However, it is clear that since

$$W_{DCB} = X_C - X_B \quad (11)$$

an increase in  $V_{CB}$  corresponds to an increase in  $W_{DCB}$  and, therefore, a decrease in the base width  $W_B$ .

#### Derivation of Early Voltage

Malone<sup>7</sup> and Malhi et. al.<sup>8</sup> derived the Early voltage  $V_A$  from the  $I_C$  versus  $V_{CE}$  curves by approximating a straight line in the forward active region and assuming an equation of the form

$$I_C = I^0 + V_{CE} \left( \frac{\partial I_C}{\partial V_{CE}} \right) \Big|_{V_{CE} = V_1} \quad (12)$$

$I^0$  is the projection of the line to  $V_{CE} = 0$  and  $V_1$  is the collector-to-emitter voltage at which the slope of the line is evaluated. The Early voltage is the projection of the trace to zero collector current. If we set  $I_C = 0$ , assume the base current  $I_B$  is constant and independent of  $V_{CE}$ , and define  $\beta_0$  as the common-emitter current gain at  $V_{CE} = 0$ , from equation (12)

$$0 = \beta_0 I_B + V_A \left( \frac{\partial I_B}{\partial V_{CE}} \right) \Big|_{V_{CE} = V_1} \quad (13)$$

and

$$V_A = -\beta_0 \left( \frac{\partial V_{CE}}{\partial \beta} \right) \Big|_{V_{CE} = V_1} \quad (14)$$

Equation (14) can be expanded by use of the chain rule<sup>12</sup> to yield

$$V_A = -\beta_0 \left( \frac{\partial V_{CE}}{\partial W_B} \right) \left( \frac{\partial W_B}{\partial \beta} \right) \Big|_{V_{CE} = V_1} \quad (15)$$

where  $\beta$  is the common-emitter gain at  $V_{CE} > 0$ . Equation (15) requires the evaluation of two derivatives, which Malone and Malhi et. al. evaluated using particular assumptions for the doping profiles in the base and collector to obtain  $V_{CE}=f(W_B)$  and  $W_B=f(\beta)$ .

Malone derived the Early voltage for a vertical pnp transistor and assumed that the collector-base junction was uniformly doped on the collector side,  $N(x)=N_c$ , and linearly graded on the base side,  $N(x)=a_b x$ . After solving Poisson's equation (2), and assuming that the collector-to-base voltage was large compared with the built-in potential of the junction ( $V_{CB} \gg \Phi_{iCB}$ ), he showed that

$$V_{CB} = q a_b X_B^3 / (3\epsilon_s) + q N_c X_C^2 / (2\epsilon_s) \quad (16)$$

where  $a_b$  is the grade constant in the base,  $N_c$  is the constant concentration in the collector, and from space charge neutrality (see equation (10)),

$$2N_c X_C = a_b X_B^2 \quad (17)$$

Malone also assumed that the emitter efficiency  $\gamma$  is essentially unity and the common-emitter current gain is limited by the base transport factor  $\alpha_T$  and, therefore,

$$\beta = 2L_{mB}^2 / W_B^2 \quad (18)$$

where  $L_{mB}$  is the diffusion length of the minority carriers in the base.

By combining equations (1), (16), (17), and (18), Malone calculated the Early

voltage to equal

$$V_A = \frac{((-qa_b XB^2 L_{mB}) / (2\epsilon_s (\beta_0/2)^{1/2})) (1 + (a_b XB / (2N_c)))}{(1 - XB / (L_{mB} \beta_0)^{1/2})^3} \quad (19)$$

Malhi et. al.<sup>8</sup> derived the Early voltage for a lateral pnp transistor and assumed that the collector was linearly graded,  $N(x) = a_c x$ , and the base uniformly doped,  $N(x) = N_b$ . The final Early voltage expression was derived similarly to Malones' and resulted in

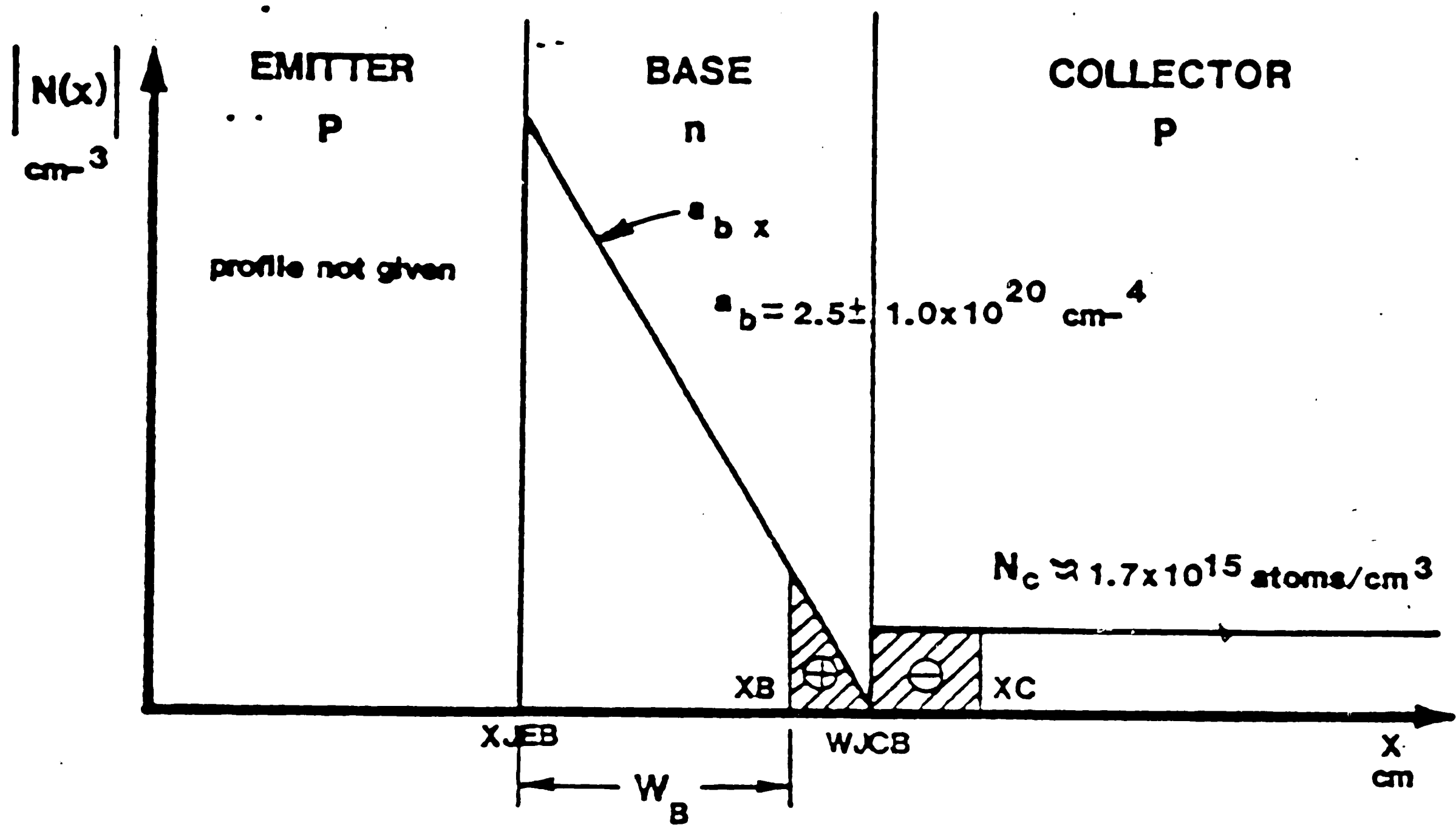
$$V_A = \frac{((qN_b L_{mB} XB) / (\epsilon_s (2\beta_0)^{1/2})) (1 + (2N_b / (a_c XB))^{1/2})}{(1 - ((\beta_0/2)^{1/2} XB / L_{mB}))^3} \quad (20)$$

Figure 3 shows the assumed profile and experimental results for the vertical pnp transistor. The grade constant  $a_b$  was experimentally determined to correlate the theory with the electrical measurements. The results indicate discrepancies at low and high betas.

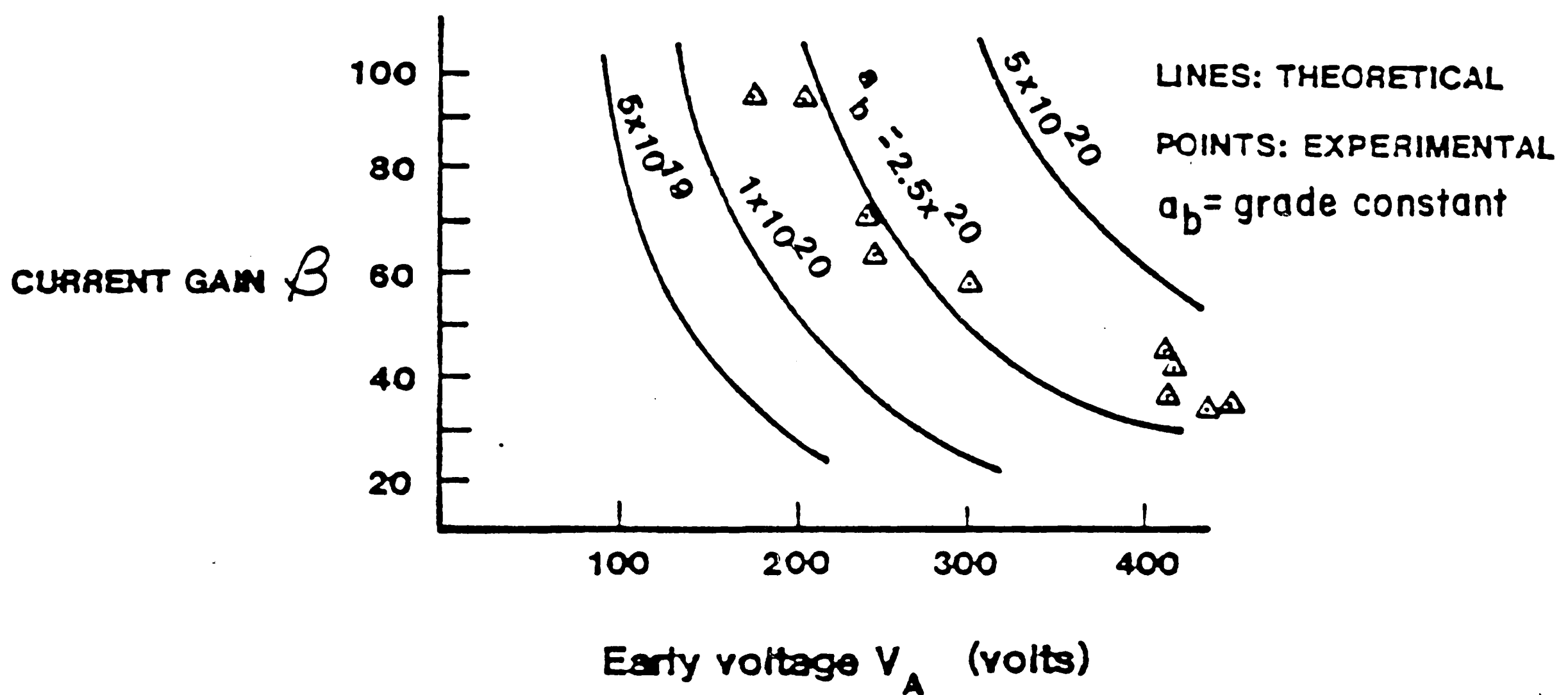
As previously mentioned, both Early voltage equations, (19) and (20), assumed specific doping profiles in the base and collector. A more exact analysis of Early voltage should not assume a particular doping profile, and should include the built-in potential of the emitter-base and collector-base junctions. The following derivation of Early voltage results from the small-signal conductance  $\partial I_C / \partial V_{CB}$  of the collector-base junction.<sup>9</sup> This final equation for Early voltage is the one used in this thesis to correlate theory with electrical measurements for npn and pnp complementary bipolar transistors.

In a bipolar transistor, the total collector current  $I_C$  is equal to<sup>11</sup>

$$I_C = (q A_E D_{mB} n_i^2 / Q_B) \exp (qV_{BE} / kT) \quad (21)$$



a. Net impurity concentration for a vertical pnp transistor – after Malone<sup>7</sup>



b. Vertical pnp Early voltage  $V_A$  versus  $\beta$  for 8 ohm-cm collector resistivity - after Malone<sup>7</sup>

Figure 3

where  $A_E$  is the area of the emitter region,  $D_{mB}$  is the minority carrier diffusion coefficient in the base,  $n_i$  is the intrinsic carrier concentration in silicon ( $n_i \cong 10^{10}$  atoms/cm<sup>3</sup> at 295 °K),  $k$  is Boltzmann's constant,  $T$  is temperature in degrees Kelvin (at room temperature  $T = 295$  °K), and  $Q_B$  is the number of doping atoms in the base per unit area.  $Q_B$  is equal to

$$Q_B = \int_0^{XB} N(x) dx \quad (22)$$

where 0 is the depletion region edge in the base at the forward biased emitter-base junction and, as stated previously,  $XB$  is the depletion region edge in the base at the reverse biased collector-base junction.

The small - signal conductance at the collector-base junction can be determined by combining equations (21) and (22) and evaluating  $\partial I_C / \partial V_{CB}$  resulting in<sup>9</sup>

$$\frac{\partial I_C}{\partial V_{CB}} = \frac{(-qD_{mB} n_i^2 A_E \exp(qV_{BE}/kT) N(XB) \partial XB / \partial V_{CB})}{\left(\int_0^{XB} N(x) dx\right)^2} \quad (23)$$

and by substituting equation (21) into (23)

$$\frac{\partial I_C}{\partial V_{CB}} = -I_C \frac{(N(XB) \partial XB / \partial V_{CB})}{\left(\int_0^{XB} N(x) dx\right)} \quad (24)$$

where

$$\frac{\partial I_C}{\partial V_{CB}} = I_C / |V_A| \quad (25)$$

An equation for Early voltage can easily be written from equations (24) and (25), and by noting that since  $W_B = XB - 0$ , and, therefore,  $\partial XB / \partial V_{CB} = \partial W_B / \partial V_{CB}$ , we obtain

$$|V_A| = \left(\int_0^{XB} N(x) dx\right) / (N(XB) \partial W_B / \partial V_{CB}) \quad (26)$$

Equation (26) is an extremely useful expression which relates the Early voltage  $V_A$  to the doping profile  $N(x)$  of the transistor. It consists of three components:

1.  $\int_0^{XB} N(x) dx$  is the area under the transistor profile in the portion of the base where transistor action is taking place - commonly referred to as the Gummel number.<sup>9</sup>

2.  $N(XB)$  is the concentration at the depletion region edge  $XB$  in the base.

3.  $\partial W_B / \partial V_{CB}$  is the derivative of the electrical base width  $W_B$  with respect to the reverse bias collector-to-base voltage  $V_{CB}$ . This is a negative number since an increase in  $V_{CB}$  causes the base width  $W_B$  ( $0 \Rightarrow XB$ ) to decrease.

The most difficult part of equation (26) is the evaluation of  $\partial W_B / \partial V_{CB}$  which requires a numerical solution to Poisson's equation (2) to obtain  $W_B = f(V_{CB})$ . A numerical technique is also required to calculate the built-in potential of the emitter-base and collector-base junctions to establish depletion region boundary conditions before a collector-to-emitter voltage is applied. The emitter-base junction potential  $\Phi_{iEB}$  must satisfy these two equations<sup>9</sup>

$$\Phi_{iEB} = (kT/q) \ln(N(XE)N(0))/n_i^2 \quad (27)$$

$$\Phi_{iEB} = q/\epsilon_s \left( \int_{XE}^0 \left( \int_x^0 N(x) dx \right) dx \right) \quad (28)$$

where  $XE$  and  $0$  are the depletion region boundaries in the emitter and base respectively. The collector-base junction potential  $\Phi_{iCB}$  must satisfy these two equations<sup>9</sup>

$$\Phi_{iCB} = (kT/q) \ln(N(XB)N(XC))/n_i^2 \quad (29)$$

$$\Phi_{iCB} = q/\epsilon_s \left( \int_{XB}^{XC} \left( \int_x^{XC} N(x) dx \right) dx \right) \quad (30)$$

where  $XB$  and  $XC$  are the depletion region boundaries in the base and collector respectively. A computer program was written to calculate the built-in potential,

Gummel number, and evaluate  $\partial W_B / \partial V_{CB}$  from the doping profile  $N(x)$ .<sup>13</sup>



### Common-Emitter Current Gain

The common-emitter current gain  $\beta$  is the incremental change of  $I_C$  with respect to an incremental change of  $I_B$  and is equal to

$$\beta = \Delta I_C / \Delta I_B = \alpha_F / (1 - \alpha_F) \quad (31)$$

where  $\alpha_F$  is the common-base current gain equal to

$$\alpha_F = \gamma \alpha_T \quad (32)$$

The base transport factor  $\alpha_T$  is the ratio of the current reaching the collector to the current injected from the emitter, and is equal to

$$\alpha_T = 1 - W_B^2 / (2L_{mB}^2) \quad (33)$$

where  $L_{mB}$  is the diffusion length of the minority carriers in the base. The emitter efficiency  $\gamma$  measures the injected minority carrier current from the emitter to the total emitter current. The common-emitter gain of modern planar transistors, operating at intermediate current levels, is mainly limited by the emitter efficiency so that to a very good approximation<sup>14</sup>

$$\beta = \beta_\gamma = \gamma / (1 - \gamma) \quad (34)$$

$$= I_{mB} / I_{mE} \quad (35)$$

where  $I_{mB}$  is the minority carrier current injected into the base from the emitter and  $I_{mE}$  is the minority carrier current injected into the emitter from the base. Equation (35) can be rewritten in terms of the doping profile  $N(x)$  and minority carrier diffusion coefficients to yield<sup>15</sup>

$$\beta_\gamma = D_{mB} \left( \int_0^{x_E} N(x) dx \right) / \left( D_{mE} \int_0^{x_B} N(x) dx \right) \quad (36)$$

$$\beta_\gamma = (D_{mB} Q_E) / (D_{mE} Q_B) \quad (37)$$

where  $D_{mB}$  and  $D_{mE}$  are the average minority carrier diffusion coefficients in the

base and emitter respectively and  $Q_E$  and  $Q_B$  are the total charges per unit area in the emitter and base respectively.

Direct evaluation of equation (37) will yield a value for  $\beta_\gamma$  several orders of magnitude higher than measured. The principal reason for this discrepancy is due to the influence of heavy doping in the emitter.<sup>14,15</sup> The main effect of heavy doping in silicon at low injection conditions is to reduce the forbidden energy gap  $E_g$ , since the doping concentrations are large enough to form an impurity band that overlaps the conduction or valence bands. A reduction in the bandgap, as a function of an increase in doping concentration  $N$ , modifies the temperature-dependent intrinsic carrier concentration  $n_i$  where

$$n_i^2 = C T^3 \exp(-E_g/kT) \quad \text{cm}^{-3} \quad (38)$$

and  $C = 5.5 \times 10^{32} / \text{cm}^3 / ^\circ\text{K}^3$  and  $E_g = 1.12 \text{ eV}$ . If we introduce an effective intrinsic carrier concentration  $n_{ie}$ , which is greater than  $n_i$ , so that

$$n_{ie}^2 = C T^3 \exp(-E_g(N)/kT) \quad \text{cm}^{-3} \quad (39)$$

and define bandgap narrowing  $\Delta E_g$  to be equal to

$$\Delta E_g = 1.12 - E_g(N) \quad \text{eV} \quad (40)$$

by combining equations (38), (39), and (40) we get

$$(n_i^2/n_{ie}^2) = \exp(-\Delta E_g/kT) \quad (41)$$

Since  $np = n_{ie}^2$ , an increase in  $n_{ie}$  implies an increase in the equilibrium minority carrier density. This results in a reduction in the emitter efficiency  $\gamma$ , since an increase in the equilibrium minority carrier density implies an increase in the injected minority carrier density at the edge of the depletion region XE in the emitter. The doping profile in the emitter is, therefore, transformed into a lower effective doping

profile  $N_{\text{eff}}(x)$  where<sup>15</sup>

$$N_{\text{eff}}(x) = N(x) n_i^2 / n_{ie}^2 \quad (42)$$

If, for example, at room temperature (295 °K) the bandgap narrowed due to heavy doping in the emitter by  $\Delta E_g = 100$  meV, the effective intrinsic carrier concentration  $n_{ie}$  would now be  $2.26 \times 10^{11} \text{ cm}^{-3}$  compared with  $n_i = 10^{10} \text{ cm}^{-3}$ . If the average concentration in the emitter  $N_{E\text{avg}}$  was equal to  $5.0 \times 10^{19} \text{ cm}^{-3}$ , the effective average emitter concentration  $N_{E\text{eff}}$  would now only be  $9.75 \times 10^{17} \text{ cm}^{-3}$ . Therefore,  $Q_E$  would lower and, consequently, reduce the calculated value of  $\beta$  by approximately 50.

There are two other effects of heavy doping which will tend to reduce the emitter efficiency  $\gamma$  (and  $\beta$ ) even further. The built-in electric field in the emitter may be in the opposite direction than expected, since the effective profile in the emitter  $N_{\text{eff}}(x)$  is smaller than the actual profile  $N(x)$ , and, therefore, aid in the flow of minority carriers from the base to the emitter. Also, since the probability of collisions between carriers is substantially increased in heavily doped silicon, there is a significant decrease in the excess carrier lifetime in the emitter due to the three-body collision (Auger) mechanism for recombination.<sup>44</sup>

Much work has been done to understand minority carrier transport in heavily doped silicon since the late 1960's; however, differences in optical and electrical measurements of bandgap narrowing, assumptions concerning the use of Maxwell-Boltzmann statistics rather than Fermi-Dirac statistics, and assumptions that minority carrier mobilities equal majority carrier mobilities have led authors to conflicting results. The following brief history of published literature on the physics

of minority carrier transport in heavily doped silicon reveals the differences in opinion among many authors and the need for additional work in this area.

In 1967, Volfson and Subashiev<sup>16</sup> presented experimental evidence that the bandgap  $E_g$  narrowed at high concentrations of impurities in silicon ( $N(x) > 2.5 \times 10^{19} \text{ cm}^{-3}$ ). Their optical measurements of the absorption edge of silicon led them to conclude that narrowing of the forbidden energy gap occurred at high doping levels in silicon. Their experimental results fit the following equation:

$$\Delta E_g = 3.4 \times 10^{-8} (N(x)^{1/3} - N_d^{1/3}) \text{ eV} \quad (43)$$

where for n-type silicon  $N_d = 1.85 \times 10^{19} \text{ cm}^{-3}$  and for p-type silicon  $N_d = 1.4 \times 10^{19} \text{ cm}^{-3}$ . Additional optical measurements of  $\Delta E_g$  by Balanski, Aziza, and Amzallag<sup>17</sup>, and Schmid<sup>18</sup> reveal similar results to Volfson and Subashiev.

In 1968, Kaufmann, Bergh, and Buhanan<sup>14</sup> theorized that the large discrepancy between calculated values of  $\beta_\gamma$  and measured  $\beta_\gamma$  was due to a bandgap decrease in the heavily doped emitter. Also in 1968, Whittier and Downing<sup>14,15</sup> postulated that the phosphorus atoms in an n-type emitter may act as very active recombination centers at doping levels higher than  $10^{19} \text{ cm}^{-3}$  which could lower the emitter charge  $Q_E$ . If the effective emitter charge  $Q_{E\text{eff}}$  is limited to the lightly doped part of the emitter, the emitter efficiency should decrease consequently lowering  $\beta_\gamma$ . In 1971, DeMan<sup>15</sup> used the measurements of Volfson and Subashiev<sup>16</sup> to obtain an effective doping profile in the emitter (see Figure 4). He modified equation (36) using equation (42) so that

$$\beta_\gamma = D_{mB} \left( \int_0^{x_E} N(x) (n_i^2/n_{ie}^2) \partial x \right) / (D_{mE} \int_0^{x_B} N(x) \partial x) \quad (44)$$

where

A THEORETICALLY CALCULATED EFFECTIVE EMITTER PROFILE  $N_{eff}(x)$  SHOWING THE DIFFERENCE IN  $Q_E$  AND  $Q_{E_{eff}}$  DUE TO BANDGAP NARROWING IN THE HEAVILY DOPED EMITTER

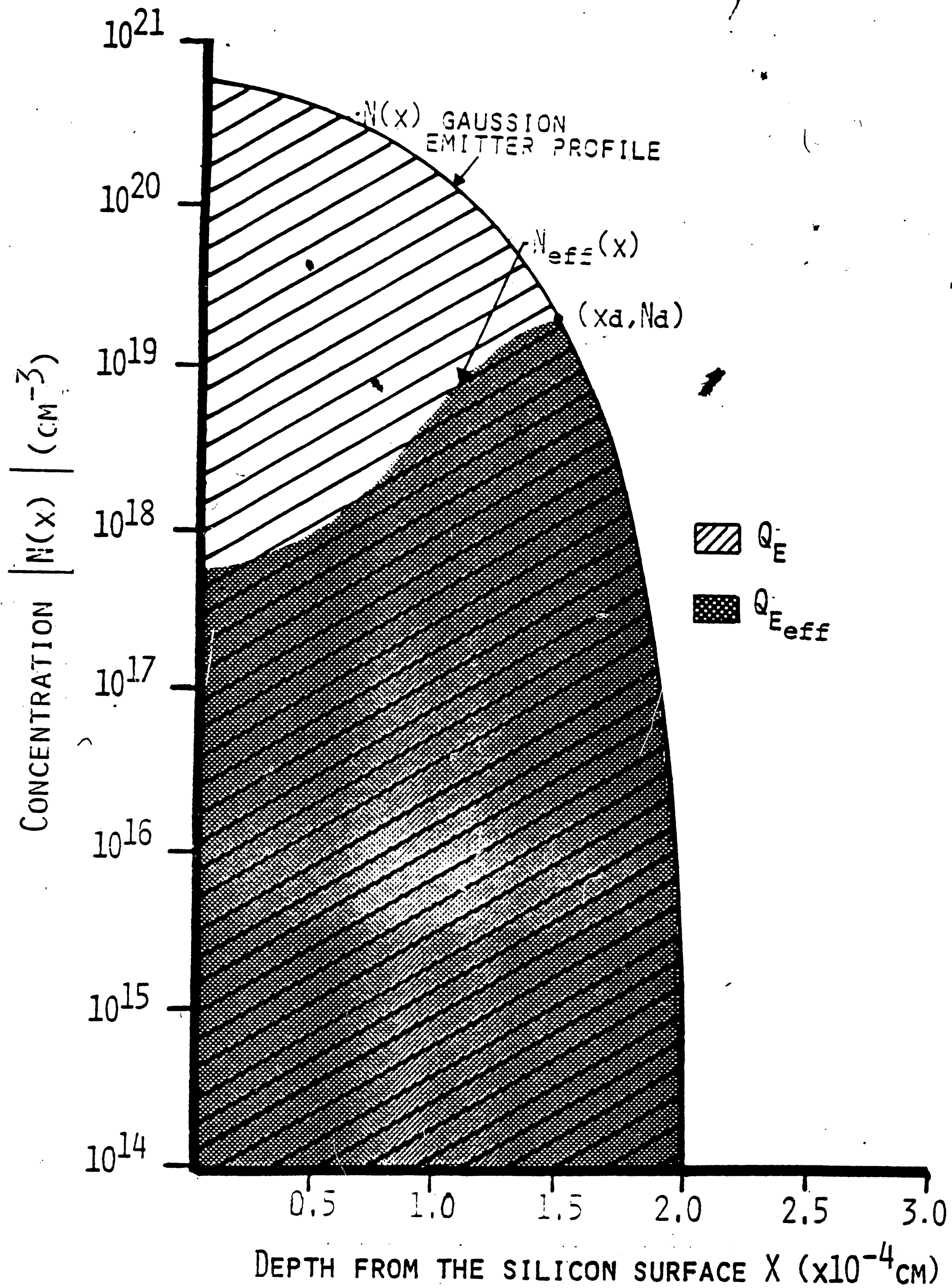


FIGURE 4

$$\begin{aligned}
N_{\text{eff}}(x) &= N(x) (n_i^2/n_{ie}^2) \\
&= N(x) \exp (-3.4 \times 10^{-8} (N(x)^{1/3} - N_d^{1/3})/kT) \quad (45)
\end{aligned}$$

DeMan's results, however, were still two to four times higher than measured. In 1977, Kleppinger and Lindholm<sup>19</sup> and Mertens, DeMan, and Van Overstraeten<sup>14</sup> indicated that due to the impurity band formation and band tailing, not only a bandgap decrease, but also a serious change in the density of states should be taken into account. Using Maxwell-Boltzmann statistics to define the effective intrinsic carrier concentration, and by deriving a theoretical effective emitter profile, Mertens et.al.<sup>14</sup> calculated values of  $\beta$  which were in much closer agreement with experimental values than DeMan's.<sup>15</sup>

In 1976, Slotboom and De Graaff<sup>20</sup> made electrical measurements of bandgap narrowing as a function of impurity concentration. They stated that at high impurity concentrations the density of states no longer has a parabolic energy distribution and becomes dependent on the impurity concentration. The bandgap is effectively reduced due to the broadening of the impurity band and the formation of band tails at the edges of the conduction band and valence band. Their measurements were done by varying base doping concentrations, assuming that the majority carrier mobilities are equal to minority carrier mobilities, and measuring the saturation current  $I_s$  from the  $I_C$  versus  $V_{BE}$  curves of a npn transistor. Their results fit the following equation:

$$\Delta E_g = E (F + (F^2 + C)^{1/2}) \text{ meV} \quad (46)$$

where  $E = 9 \text{ meV}$ ,  $F = \ln N/N_0$ ,  $N = \text{average impurity concentration}$ , and  $C = 0.5$ . These results differed considerably from Volfson and Subashiev's.<sup>16</sup>



Slotboom and De Graaff explained this discrepancy due to the fact that the optical absorption measurements of Volfson and Subashiev involved the energy gap between two free levels which can be larger than the bandgap that determines the  $pn = n_{ie}^2$  product. In 1980, Weider<sup>21</sup> determined  $\Delta E_g$  for heavily arsenic doped silicon and his measurements agreed quite well with Slotboom and De Graaff. Also, Tang<sup>22</sup> investigated heavy doping in pnp bipolar transistors and his data suggested that  $\Delta E_g$  for boron-doped silicon is not much different than arsenic-doped and phosphorus-doped silicon. In 1982, Dhariwal and Ojha<sup>23</sup> provided a theoretical basis to the empirical results of Slotboom and De Graaff. Using Maxwell-Boltzmann statistics their theoretical results agreed very well with Slotboom and De Graaff.

In 1978, Stojadinovic and Ristic<sup>24</sup> theorized that mechanical stress in the silicon lattice, due to the misfit of a high concentration of impurity atoms, may enhance the bandgap narrowing effect. They believed that the total bandgap narrowing in the emitter region was due to the modification of the energy band structure and a change in the density of states, as well as lattice stress where

$$\Delta E_{g_{\text{stress}}} = \alpha \xi E_y N_E / (1-\nu) \quad (47)$$

and

$\alpha$  is the coefficient of bandgap energy stress ( $7.5 \times 10^{-12}$  eV cm<sup>2</sup>/dyn),  $\xi$  is the silicon lattice contraction coefficient ( $10^{-24}$  cm<sup>3</sup> phosphorus,  $5.2 \times 10^{-24}$  cm<sup>3</sup> boron),  $E_y$  is Young's modulus of silicon ( $1.9 \times 10^{12}$  dyn/cm<sup>2</sup>),  $\nu$  is Poisson's ratio of silicon (0.27), and  $N_E$  is the average impurity concentration in the emitter. If equation (47) is evaluated for high emitter doping concentrations, however,

$\Delta E_{g_{\text{stress}}}$  is only a small percentage ( 4-5 %) of the total band gap narrowing measured by Slotboom and De Graaff.

In 1982, Neugroschel, Pao, and Lindholm<sup>25</sup> experimentally determined  $\Delta E_g$  by measuring recombination current in heavily doped silicon. They maintained that earlier work<sup>20,21</sup> underestimated bandgap narrowing and they used Fermi-Dirac statistics to describe the degenerate electron concentration in the conduction band. They indicated that  $\Delta E_g$  is not a function of temperature in the temperature range investigated and that the values of  $\Delta E_g$  deduced are insensitive to the mechanisms controlling recombination and the value of minority carrier mobility. They predicted much higher values of  $\Delta E_g$  than Slotboom and De Graaff.<sup>20</sup> Neugroschel et. al. made the following assumptions: 1.)  $N(x)$  is constant in the emitter, 2.) all impurities are fully ionized at the temperature used in their experiments, 3.) the density of states retains the square root dependency on energy. The data of Neugroschel et.al. showed values of  $\Delta E_g$  50-60 meV higher than previously reported. In 1983, Lee and Fossum<sup>26</sup> provided a theoretical basis for the discrepancy in optical and electrical measurements of bandgap narrowing. Their theoretical predictions agreed quite well with measurements previously reported. In 1984, Del Alamo and Swanson<sup>27</sup> maintained that due to the narrow temperature range Neugroschel et. al. overestimated  $\Delta E_g$ . They revealed that if temperature dependence of  $\Delta E_g$  is included in the calculations of Neugroschel et.al., the results of Neugroschel et. al. can be modified to agree quite well with Slotboom and De Graaff.

Besides determining  $\Delta E_g$ , values of minority carrier mobilities (which are



related to minority carrier diffusion coefficients through the Einstein relation  $(D/\mu)=(kT/q)$  must be used to calculate  $\beta_{\gamma}$ . In 1979, Dziewior and Silber<sup>28</sup> determined the minority carrier diffusion coefficients in phosphorus and boron doped silicon by measuring the complex diffusion length of minority carriers generated by a 10.7 MHz optical excitation. Their measurements indicated that for impurity concentrations ranging from  $10^{17} \text{ cm}^{-3}$  to  $10^{19} \text{ cm}^{-3}$  the minority hole mobility is slightly higher than the majority hole mobility and the minority electron mobility agrees quite well with the majority electron mobility. In 1984, Burk and De La Torre<sup>29</sup> obtained an empirical fit for minority hole mobilities. Their results agreed with Dziewior and Silber. However, Burk and De La Torre also showed that the minority hole mobility is lower than the majority hole mobility for impurity concentrations greater than  $2 \times 10^{19} \text{ cm}^{-3}$ . They modified Muller and Kamins<sup>9</sup> expression for majority hole mobility to account for the minority hole mobility difference. The mobility equations of Muller and Kamins, and Burk and De La Torre are given below:

Muller and Kamins<sup>9</sup> - majority mobilities

$$\mu = \mu_{\min} + (\mu_{\max} - \mu_{\min}) / (1 + (N/N_{\text{ref}})^{\alpha}) \text{ cm}^2/\text{v sec} \quad (48)$$

	electrons	holes
$\mu_{\min}$	92	47.7
$\mu_{\max}$	1360	495
$N_{\text{ref}}$	$1.3 \times 10^{17} \text{ cm}^{-3}$	$6.3 \times 10^{16} \text{ cm}^{-3}$
$\alpha$	0.91	0.76

and

Burk and De La Torre<sup>29</sup> - minority hole mobilities

$$\mu_p = \mu_{\min} + (\mu_{\max} - \mu_{\min}) / (1 - (N/N_{\text{ref1}})^{\alpha_1}) - \mu_{\text{add}} / (1 + (N_{\text{ref2}}/N)^{\alpha_2}) \text{ cm}^2/\text{v sec} \quad (49)$$

where  $\mu_{\min} = 6.07$ ,  $\mu_{\max} = 495$ ,  $\mu_{\text{add}} = 277$ ,  $N_{\text{ref1}} = 1.63 \times 10^{18} \text{ cm}^{-3}$ ,  $N_{\text{ref2}} = 1.16 \times 10^{23} \text{ cm}^{-3}$ ,  $\alpha_1 = .797$ ,  $\alpha_2 = .550$ . No data was provided for minority electron mobilities so it will be assumed that Muller and Kamins expression for majority electron mobilities holds true for minority electron mobilities.

In 1985, Fossum, Burk, and Yung<sup>30</sup> attempted to correlate measurements of minority carrier mobility<sup>28,29</sup> and electrical energy gap narrowing. They suggested a model for effective minority carrier mobility based on trapping of carriers in shallow (band-tail) states. Their data estimated  $\Delta E_g$  to be 25-50 meV smaller than previously published data<sup>26</sup> and they stated three reasons to question the accuracy of previous data: 1.) assumptions that minority hole mobilities equal the majority hole mobilities, 2.) assumptions that all impurities are ionized at high concentrations of impurities, and 3.) ignoring the temperature dependence of mobility and  $\Delta E_g$ .

Bennett<sup>31</sup> disagrees with Burk and De La Torre and he maintains that for impurity concentrations greater than  $10^{19} \text{ cm}^{-3}$  holes (electrons) scatter differently from donors (acceptors) than from acceptors (donors) because repulsive and attractive potentials of the same strength do not scatter equally. At high impurity concentrations, minority carriers are scattered less by dopant ions than the majority carriers, and therefore, minority carriers should have larger mobilities whenever carrier-dopant ion scattering dominates ( $N(x) > 10^{19} \text{ cm}^{-3}$ ). Bennett's theoretical analysis indicated that for impurity concentrations between  $2 \times 10^{19} \text{ cm}^{-3}$  and  $8 \times$

$10^{19} \text{ cm}^{-3}$ .

$$(\text{minority hole mobility} / \text{majority hole mobility}) \cong 3.0 \quad (50)$$

and

$$(\text{minority electron mobility} / \text{majority electron mobility}) \cong 1.2 \quad (51)$$

Bennett<sup>32</sup> also disagrees with Fossum et al. and Slotboom and De Graaff and he theoretically predicts bandgap narrowing only at impurity concentrations of  $10^{20} \text{ cm}^{-3}$  and higher. Using a quantum description of bandgap narrowing, Bennett obtained the following theoretical equation for  $10^{19} \text{ cm}^{-3} < N(x) < 3 \times 10^{20} \text{ cm}^{-3}$ :

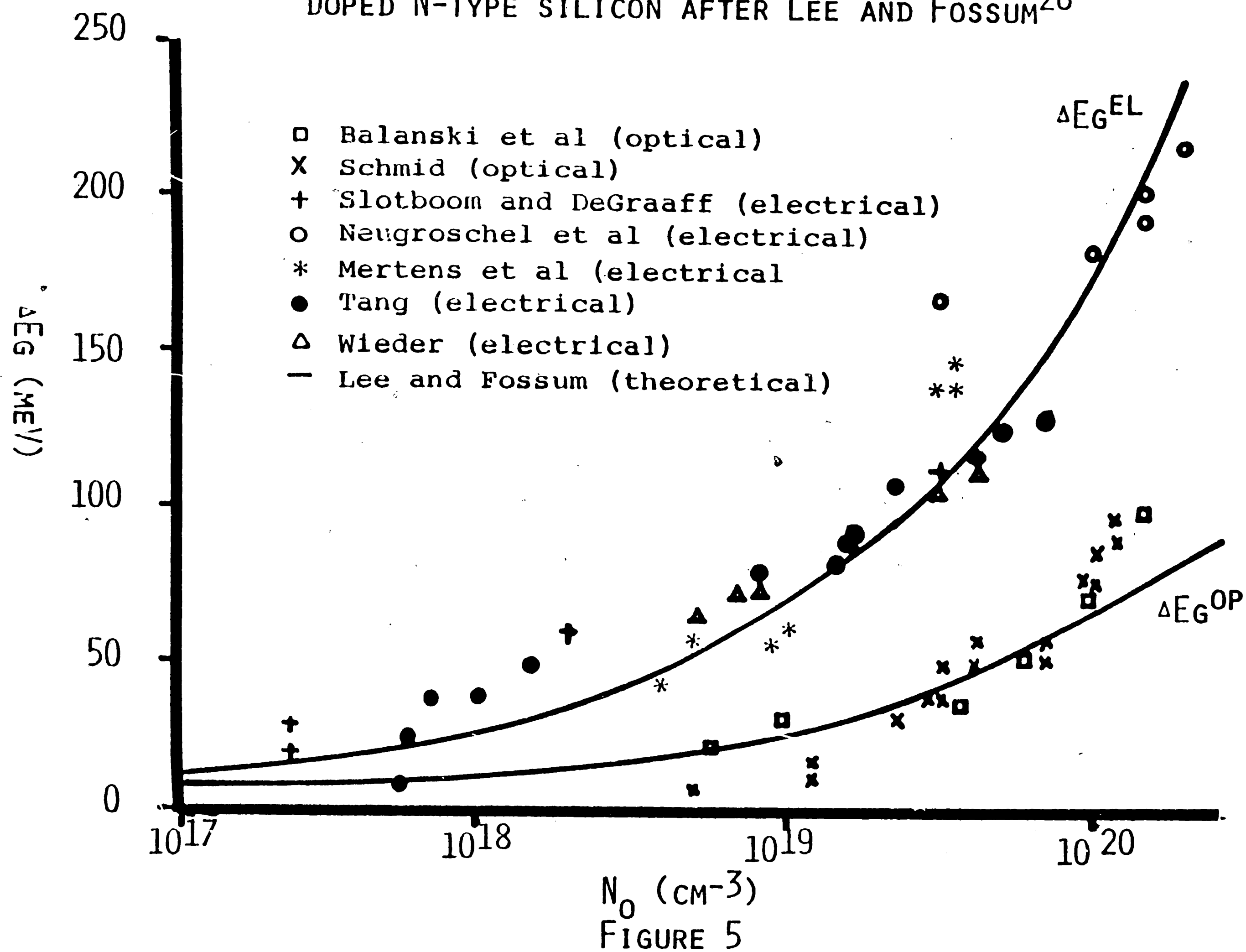
$$(n_{ie}/n_i) = 1 + 1.9 \exp(-(|N(x) - N_D|/N_n)^3) \quad (52)$$

where  $N_D = 2.4 \times 10^{20} \text{ cm}^{-3}$  and  $N_n = 1.68 \times 10^{20} \text{ cm}^{-3}$ .

Figures 5 and 6 are plots of various theoretical and experimental results of bandgap narrowing and minority hole mobilities.

ELECTRICAL  $\Delta E_G^{EL}$  AND OPTICAL  $\Delta E_G^{OP}$  BANDGAP NARROWING MEASUREMENTS VERSUS DOPING CONCENTRATION IN HIGHLY DOPED N-TYPE SILICON AFTER LEE AND FOSSUM<sup>26</sup>

28



$N_0$  ( $cm^{-3}$ )  
FIGURE 5

MAJORITY AND MINORITY HOLE MOBILITIES  
VERSUS CONCENTRATION N

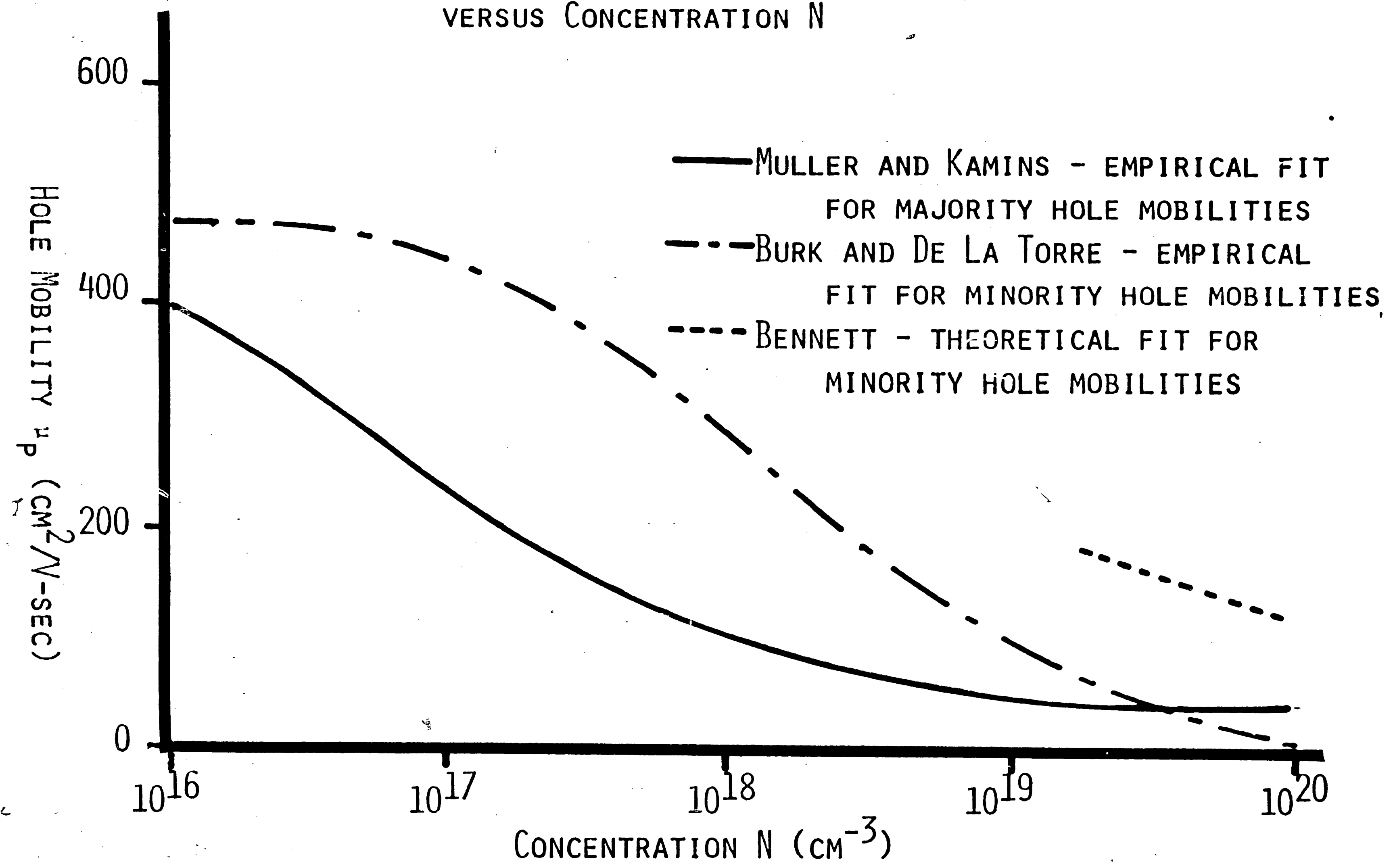


FIGURE 6

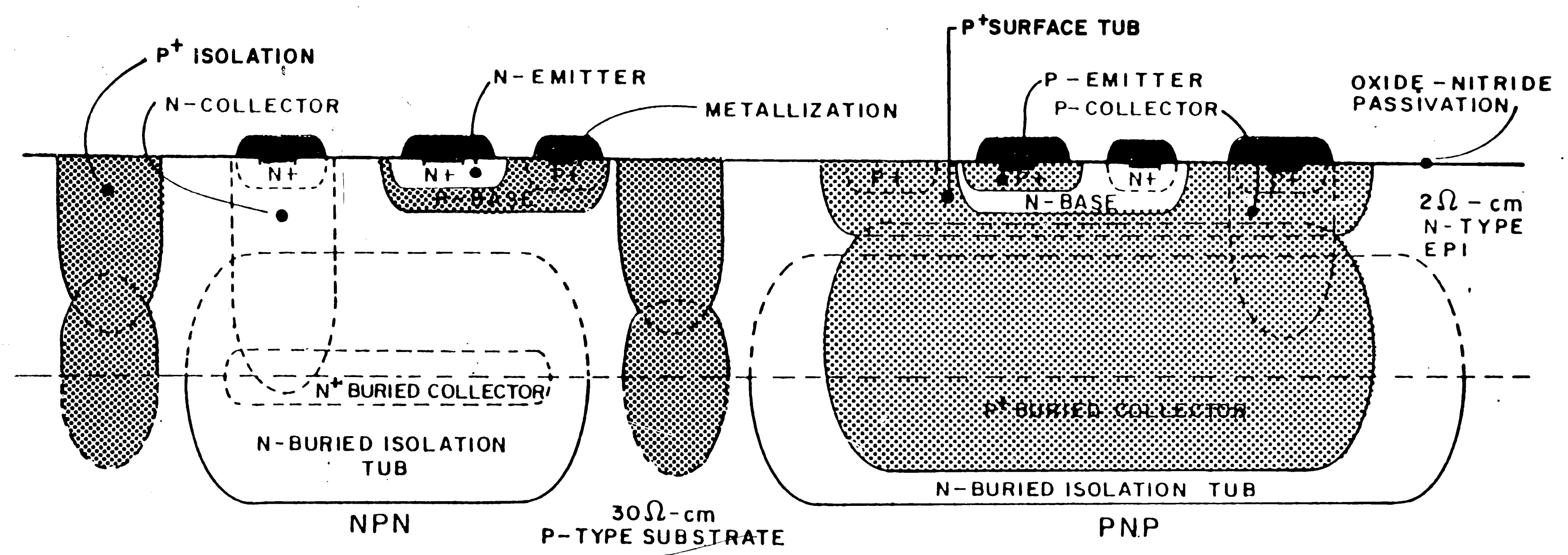
### III. EXPERIMENTAL BACKGROUND

#### Overview of Complementary Bipolar Processing Technology

The Complementary Bipolar Integrated Circuit (CBIC) process was first described in 1972.<sup>33</sup> This process allows for the fabrication of both vertical npn and vertical pnp transistors with nearly identical electrical characteristics. Unlike the traditional Standard Buried Collector (SBC) process which produces npn transistors of high performance (typically  $\beta \sim 200$  and  $f_T \sim 500$  MHz) and lateral pnp transistors of relatively poor performance (typically  $\beta \sim 50$  and  $f_T \sim 5$  MHz), CBIC structures contain both high performance npn and pnp transistors (typically  $\beta \sim 80-100$  and  $f_T \sim 450$  MHz).<sup>34</sup> Low voltage ion implant predepositions rather than diffusion sources are required in the CBIC process to obtain precise doping profiles. This precision is necessary to achieve consistently high breakdown voltages, high betas, and low series collector resistances.<sup>35</sup>

The structure of the basic CBIC npn and pnp transistors is shown in Figure 7. The substrate is p-type containing three buried layers upon which an n-type epitaxial layer is grown. The lightly doped n-type buried isolation tub is under the pnp transistor to isolate the collector of the pnp from the substrate. The buried isolation tub also serves to lower the collector-substrate parasitic capacitance of the npn. The  $p^+$  buried layer diffuses up and crosses the pnp collector surface tub diffusing down. This crossover forms a totally self-isolated p-type tub with low series resistance for the collector of the pnp. The  $n^+$  buried layer serves to lower the series collector resistance of the npn. The subsequent npn and pnp process steps are interlaced such that a specific diffusion layer (e.g. base) is first processed for the

31



CBIC device structure.

 P-TYPE

FIGURE 7

pn<sub>p</sub> and then for the npn. The junction isolation for resistors, npn transistors, and capacitors is achieved by the p<sup>+</sup> buried layer up-diffusing and crossing a p<sup>+</sup> surface tub down-diffusing. A p<sup>+</sup> (npn base) surface ring surrounds the pnp transistor to prevent the n base of the pnp from shorting to the epitaxial layer.<sup>35</sup>

#### Electrical Measurements of Complementary Bipolar Transistors

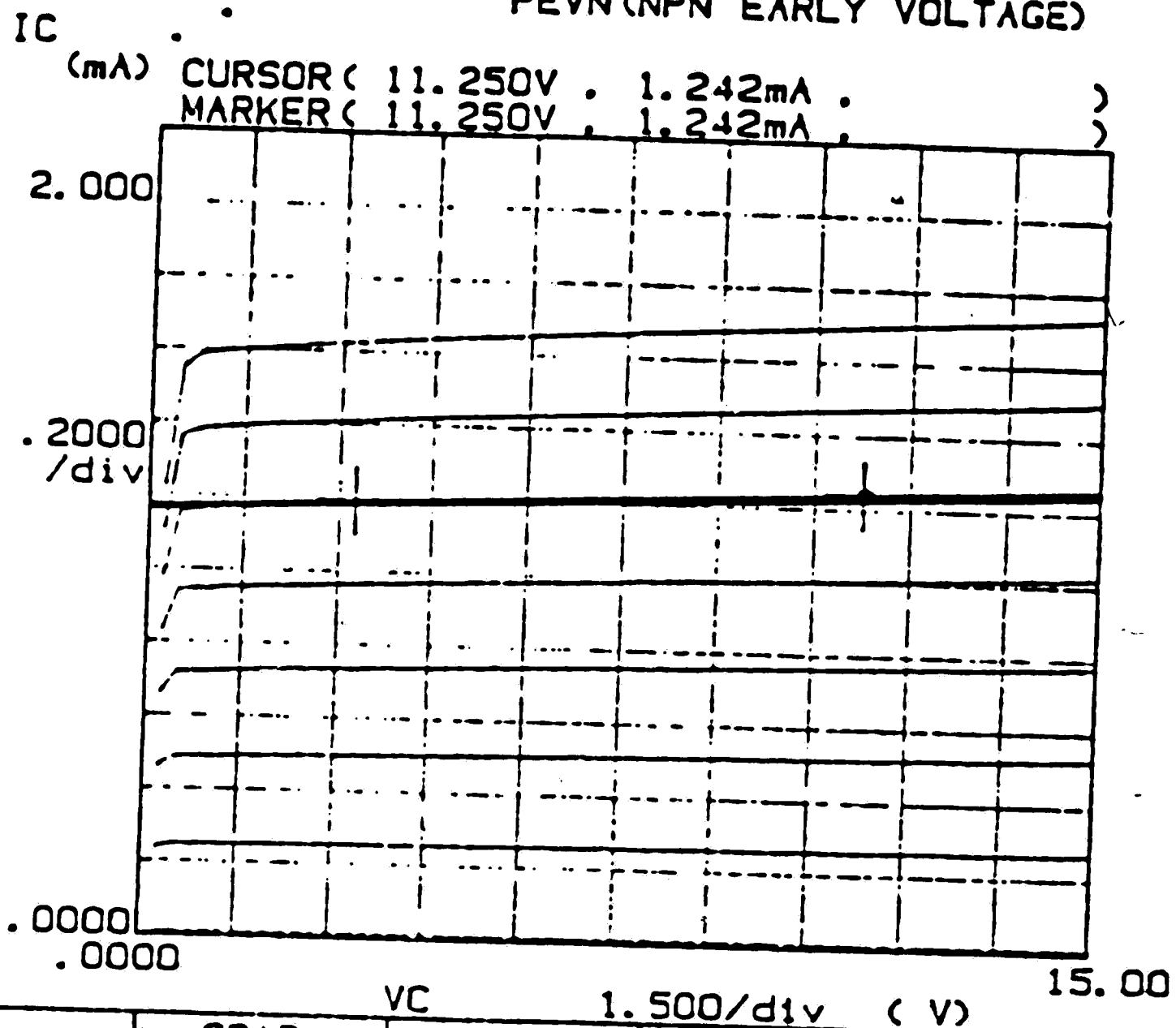
The Early voltage  $V_A$  was measured as the x-intercept on the  $V_{CE}$  axis from the slope of a line drawn on the  $I_C$  versus  $V_{CE}$  curves at  $I_B = 10 \mu A$  (see Figure 8). Care was taken to make sure that the line drawn was on the flat portion of the curves (active region,  $V_{CE} \gg 0.7$  v)) so as to not include saturation. The common-emitter current gain  $\beta$  was measured from the  $\beta$  versus  $I_C$  curves at  $I_C = 1$  mA and  $V_{CB} = 2.5$  volts (see Figure 9). Also, the saturation current  $I_S$  was measured from the extrapolation to  $V_{BE} = 0$  volts of the  $I_C$  versus  $V_{BE}$  curves (see Figure 10). Table I summarizes the electrical measurements for both CBIC npn and pnp transistors.

TABLE I

	$I_S$ ( $\times 10^{-16}$ A)	$ V_A $ (volts)	$\beta$
<b>nnp</b>	1.72	191.0	119
<b>pnp</b>	1.34	74.2	103



\*\*\*\*\* GRAPHICS PLOT \*\*\*\*\*  
PEVN (NPN EARLY VOLTAGE)



Variable1:  
VC -Ch1  
Linear sweep  
Start .0000V  
Stop 15.000V  
Step .2500V

Variable2:  
IB -Ch4  
Start 100.0nA  
Stop 14.10uA  
Step 2.000uA

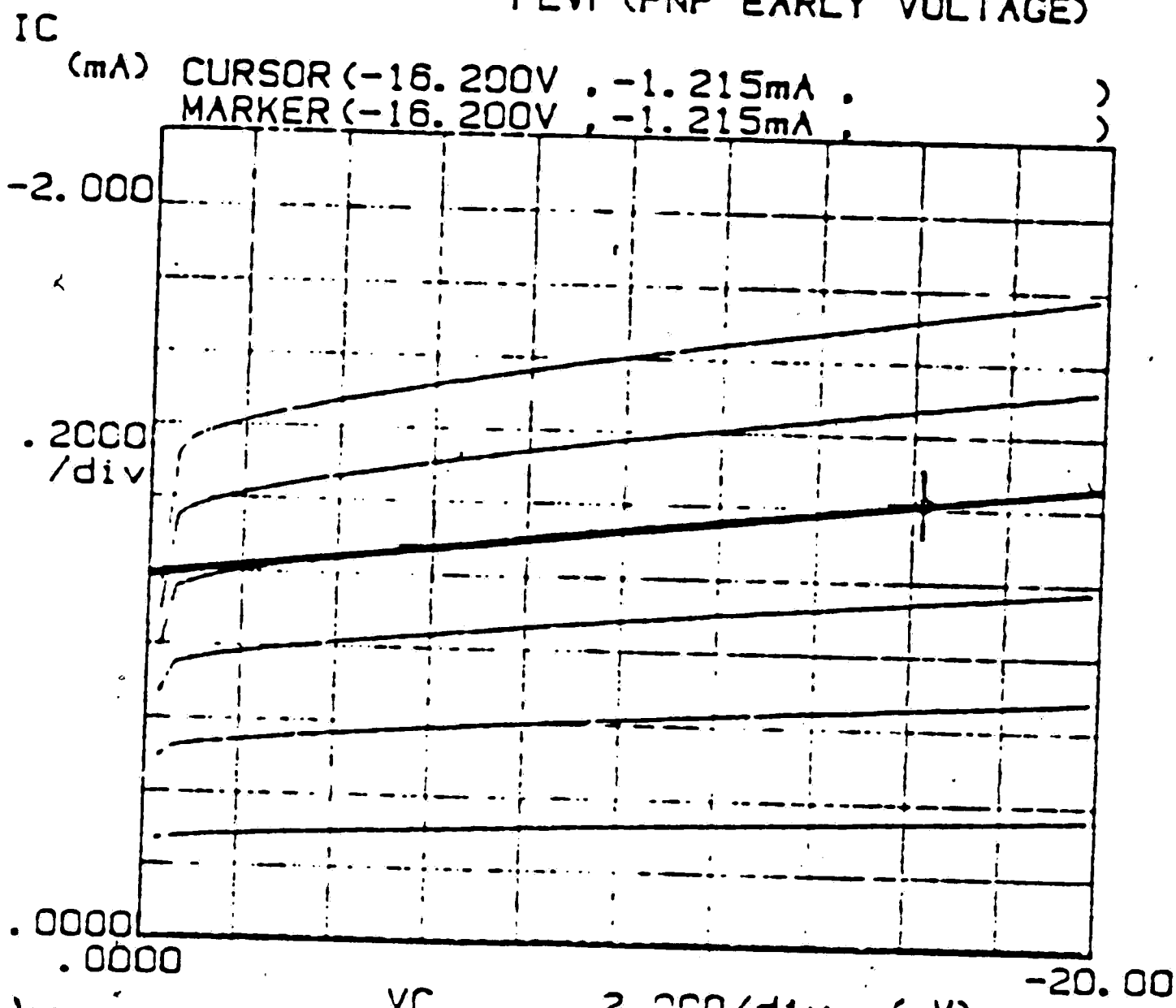
Constant1:  
VE -Ch3 .0000V

NPN

$$|V_A| = 191$$

	GRAD	1/GRAD	Xintercept	Yintercept
LINE1	6.12E-06	163E+03	-191E+00	1.17E-03
LINE2				

\*\*\*\*\* GRAPHICS PLOT \*\*\*\*\*  
PEVP (PNP EARLY VOLTAGE)



Variable1:  
VC -Ch1  
Linear sweep  
Start .0000V  
Stop -20.000V  
Step -.3000V

Variable2:  
IB -Ch4  
Start -100.0nA  
Stop -15.10uA  
Step -2.500uA

Constant1:  
VE -Ch3 .0000V

PNP

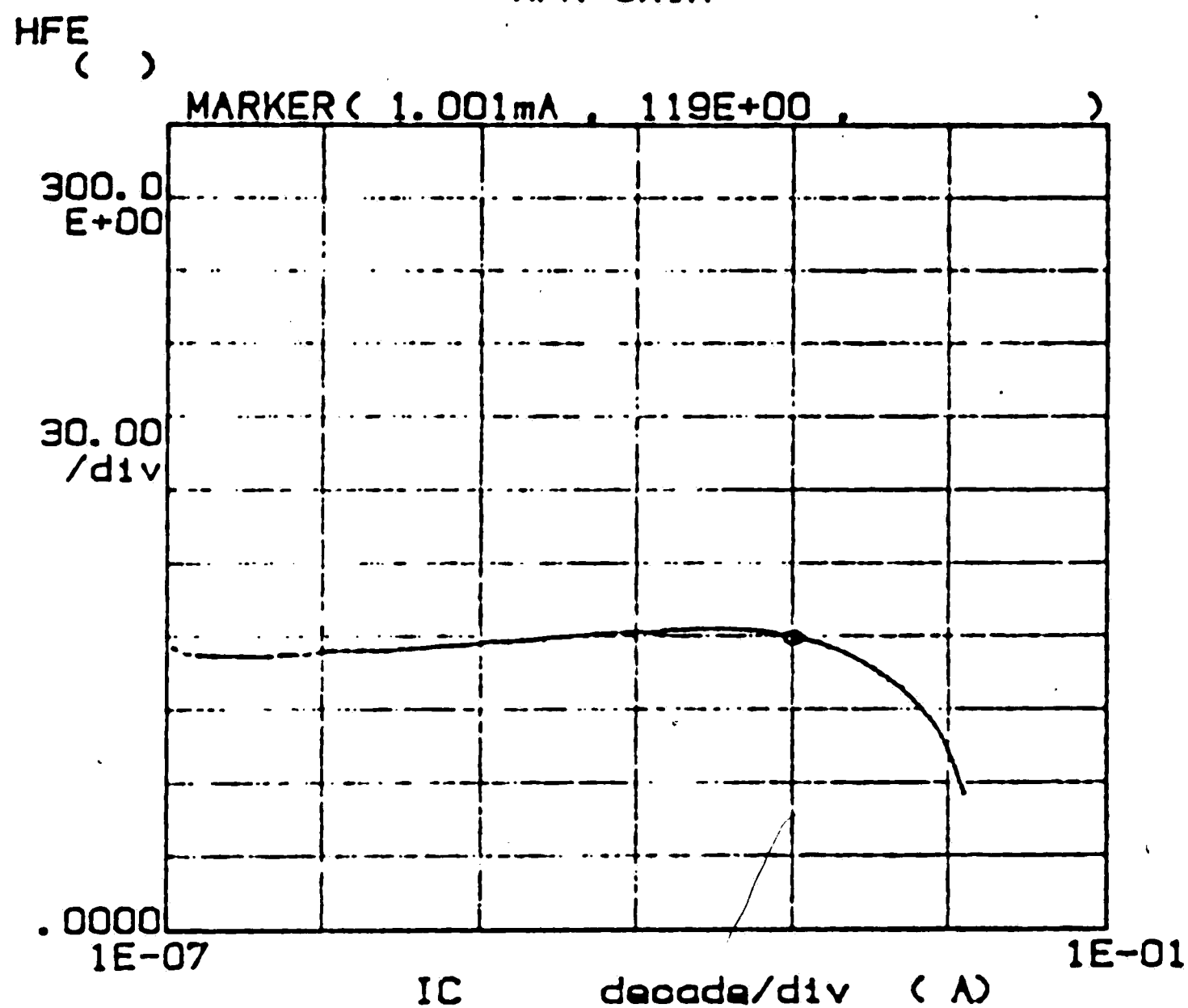
$$|V_A| = 74.2$$

	GRAD	1/GRAD	Xintercept	Yintercept
LINE1	13.4E-06	74.5E+03	74.2E+00	-997E-06
LINE2				

ELECTRICAL MEASUREMENTS OF  $I_C$  VERSUS  $V_{CE}$   
FOR CBIC NPN AND PNP TRANSISTORS

FIGURE 8

\*\*\*\*\* GRAPHICS PLOT \*\*\*\*\*  
NPN GAIN

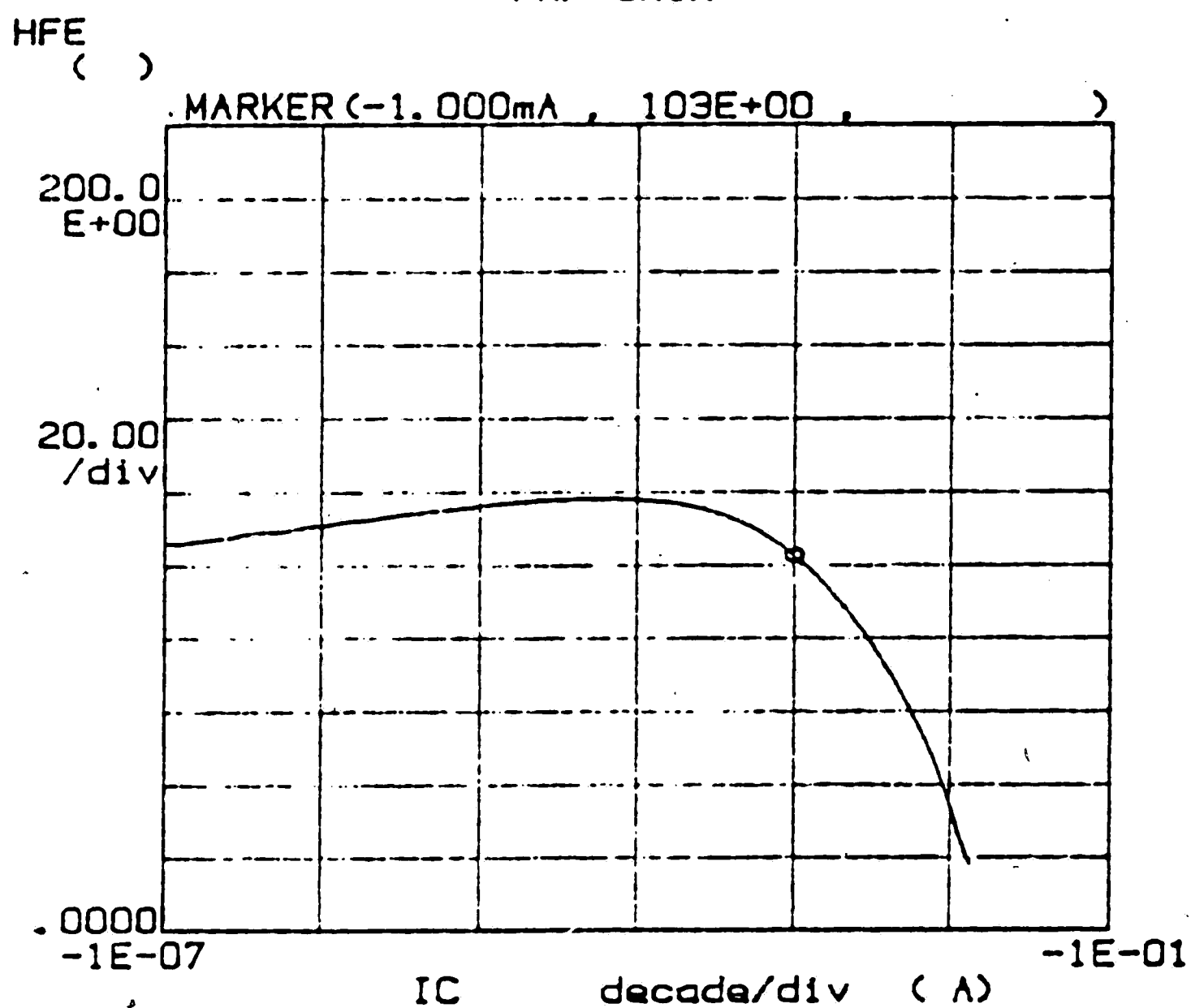


Variables:  
VE -Ch3  
Linear sweep  
Start -.5000V  
Stop -.9000V  
Step -.0050V

Constants:  
VC -Ch1 2.5000V  
VB -Ch4 .0000V

NPN  
 $\beta = 119$

\*\*\*\*\* GRAPHICS PLOT \*\*\*\*\*  
PNP GAIN



Variables:  
VE -Ch3  
Linear sweep  
Start .5000V  
Stop 1.0000V  
Step .0050V

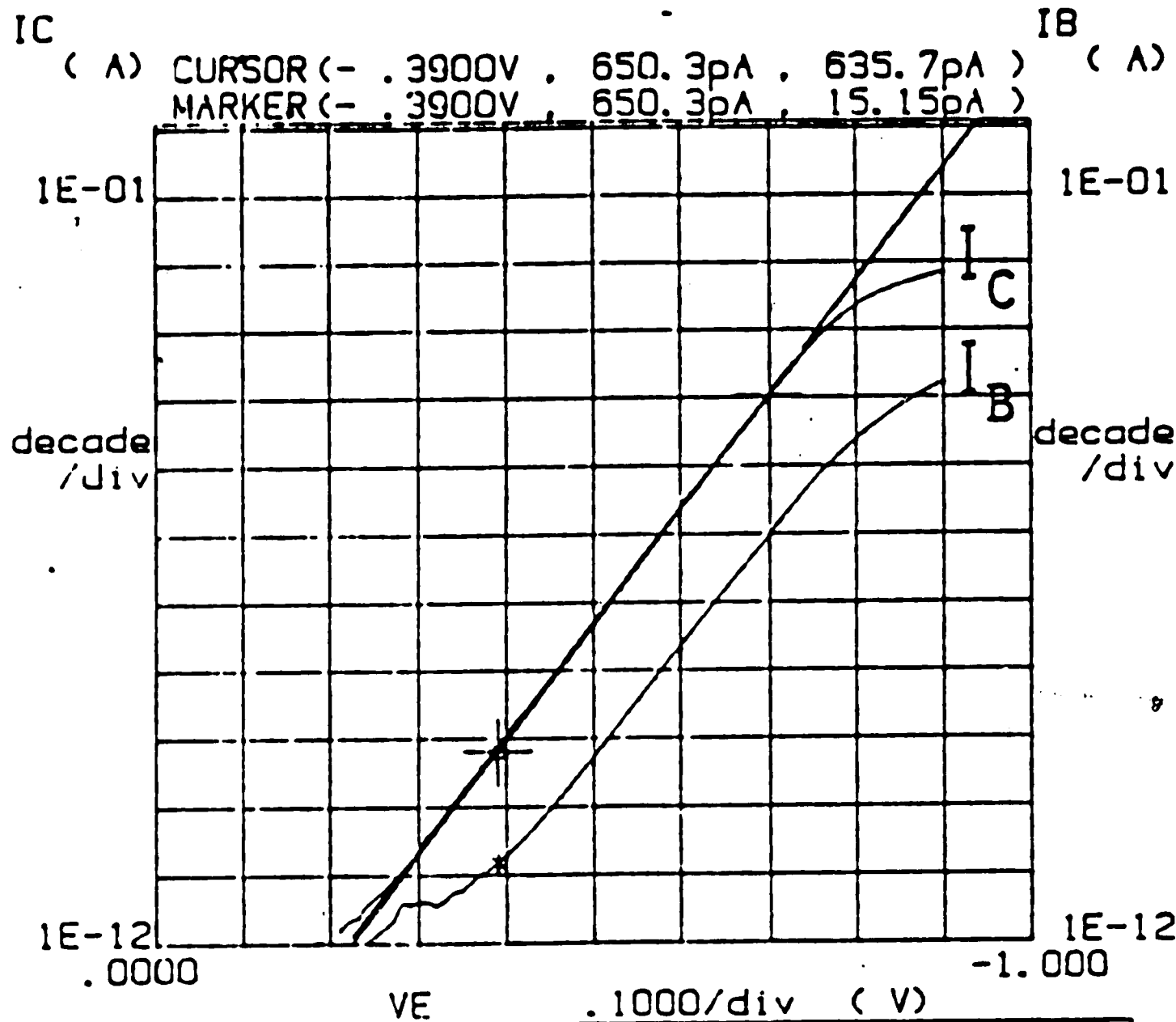
Constants:  
VC -Ch1 -2.5000V  
VB -Ch4 .0000V

PNP  
 $\beta = 103$

ELECTRICAL MEASUREMENTS OF  $\beta$  VERSUS  $I_C$   
FOR CBIC NPN AND PNP TRANSISTORS

FIGURE 9

\*\*\*\*\* GRAPHICS PLOT \*\*\*\*\*  
 PICIBN (IS @ VBE - 0)



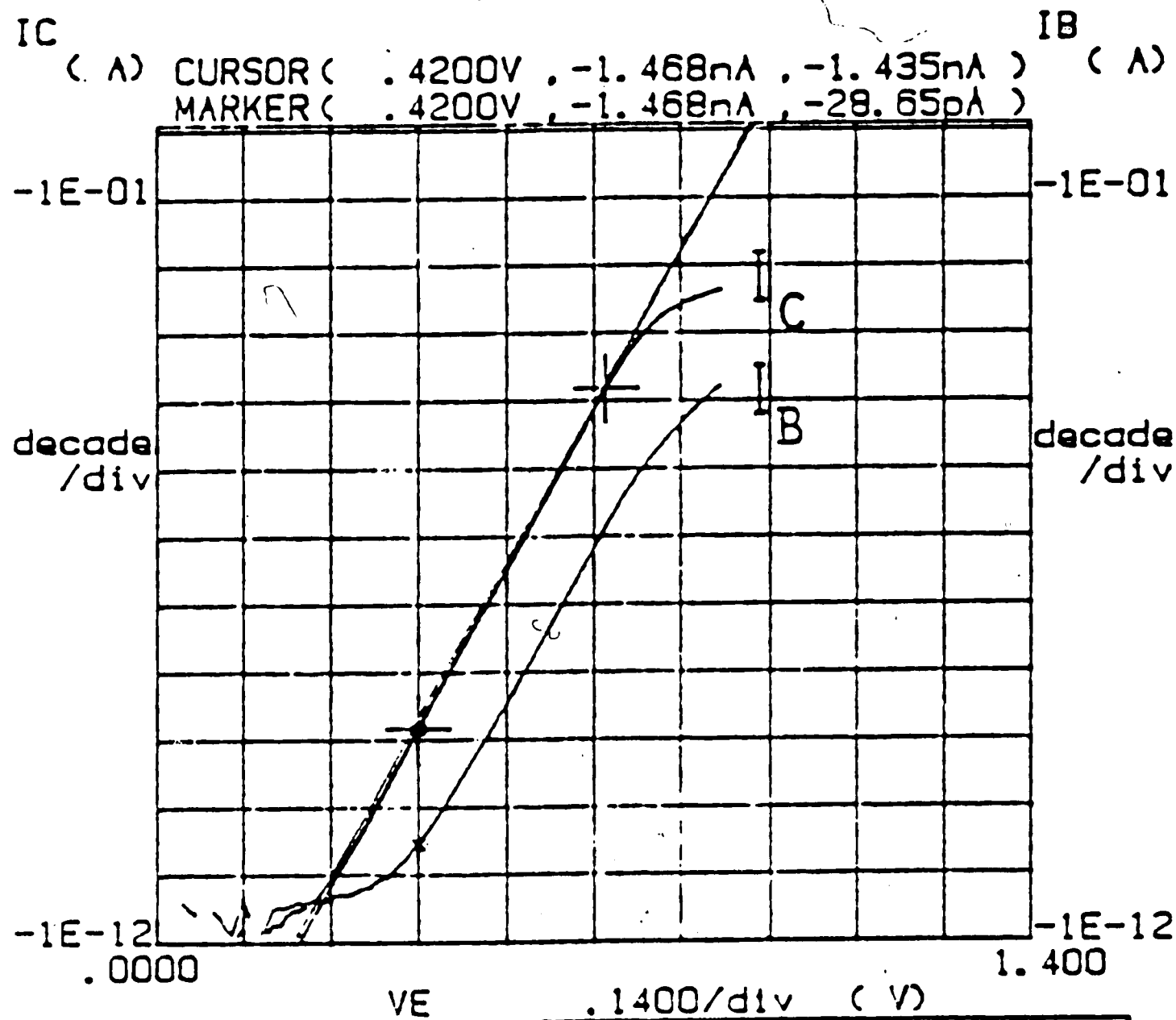
Variables:  
 VE -Ch1  
 Linear sweep  
 Start .0000V  
 Stop -.9000V  
 Step -.0100V

Constants:  
 VB -Ch2 .0000V  
 VC -Ch3 .0000V

NPN  
 $I_S = 1.72 \times 10^{-16} A$

	GRAD	1/GRAD	Xintercept	Yintercept
LINE1	-16.9E+00	-59.3E-03	-935E-03	172E-18
LINE2				

\*\*\*\*\* GRAPHICS PLOT \*\*\*\*\*  
 PICIBP (IS @ VBE-0)



Variables:  
 VE -Ch1  
 Linear sweep  
 Start .0000V  
 Stop .9000V  
 Step .0100V

Constants:  
 VB -Ch2 .0000V  
 VC -Ch3 .0000V

PNP  
 $I_S = 1.34 \times 10^{-16} A$

	GRAD	1/GRAD	Xintercept	Yintercept
LINE1	16.8E+00	59.7E-03	947E-03	-134E-18
LINE2				

ELECTRICAL MEASUREMENTS OF  $I_C$  AND  $I_B$   
 VERSUS  $V_{BE}$  FOR CBIC NPN AND PNP TRANSISTORS

FIGURE 10

### Discussion of Diffusion Profile Measurement Techniques

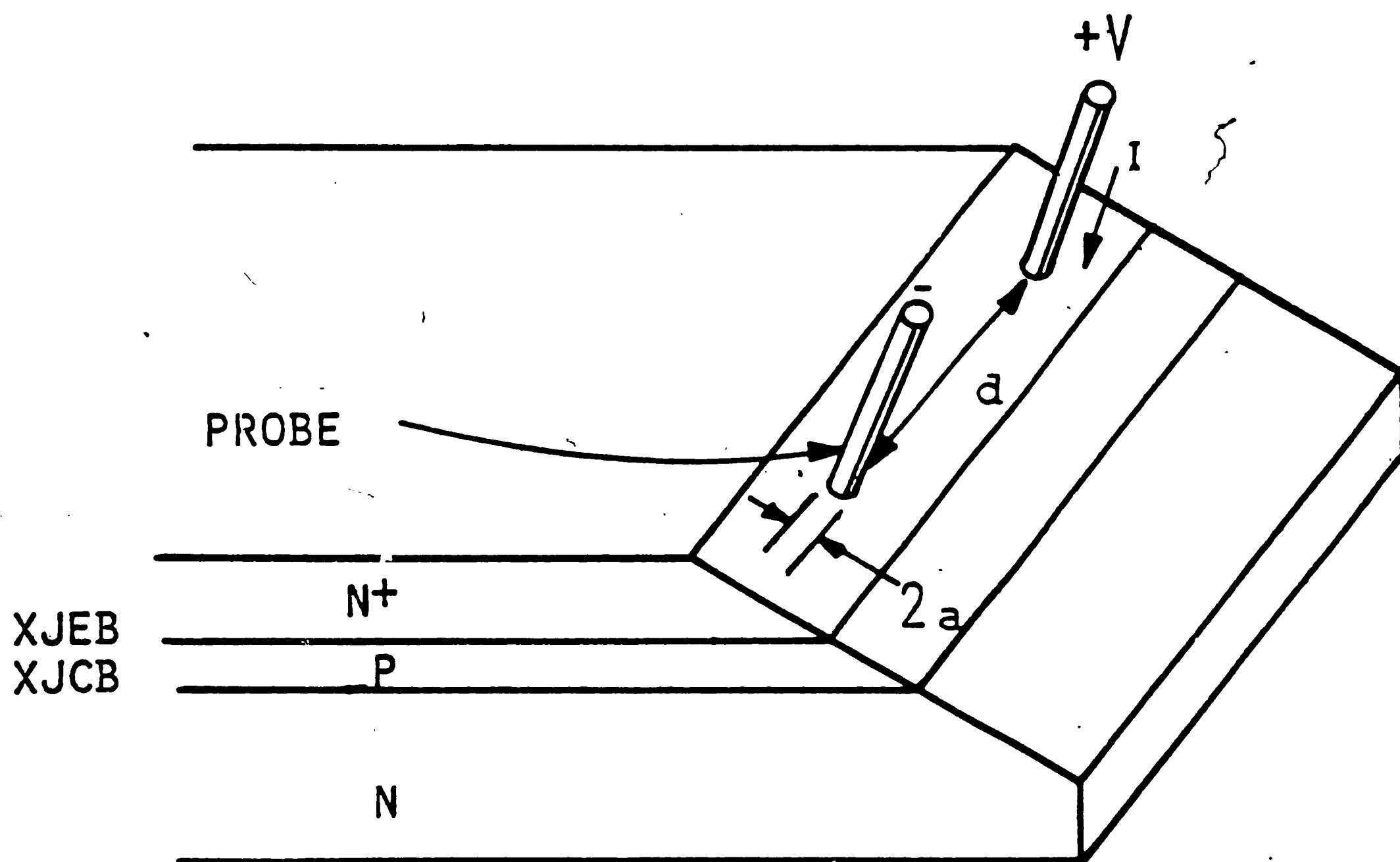
To analyze the CBIC npn and pnp transistor structures various measurement techniques were performed. These techniques included: spreading resistance profiling (SRP), angle-lap and staining, and van der Pauw sheet resistance measurements.

#### Spreading Resistance Profiling (SRP)

This technique determines the electrically active dopant profile of the transistor. SRP measurements involve contacting a precisely bevelled sample with two probes of a given radius  $a$  and a separation distance  $d$ . When a voltage is applied across the probes, the current through the probes is measured (see Figure 11).<sup>36</sup> The resistance  $R_m$  obtained includes both the resistance of the semiconductor  $R_s$  and the contact resistance of the probe tip-to-silicon surface  $R_{con}$ . For a flat circular contact of radius  $a$ <sup>37</sup>

$$R_m = R_s + R_{con} = \rho / (4a) \quad (53)$$

where  $\rho$  is the resistivity of the semiconductor material. Rather than solving equation (53) explicitly, the usual procedure is to measure  $R_m$  for several known resistivities of homogenous material with the same crystal orientation and prepare a calibration curve. Once the resistivity is known, the concentration can be determined by the use of Irvin's curves as described in the National Bureau of Standards - Special Publication 400-4. From this method, it is apparent the spreading resistance is a comparison technique and depends upon the accuracy of a calibration curve and reproducing the same measurement conditions each time a SRP is performed. This means constant attention to the condition of the probe tips and monitoring the probe



A BEVELLED SAMPLE OF AN NPN TRANSISTOR  
 PREPARED FOR SPREADING RESISTANCE MEASUREMENTS.

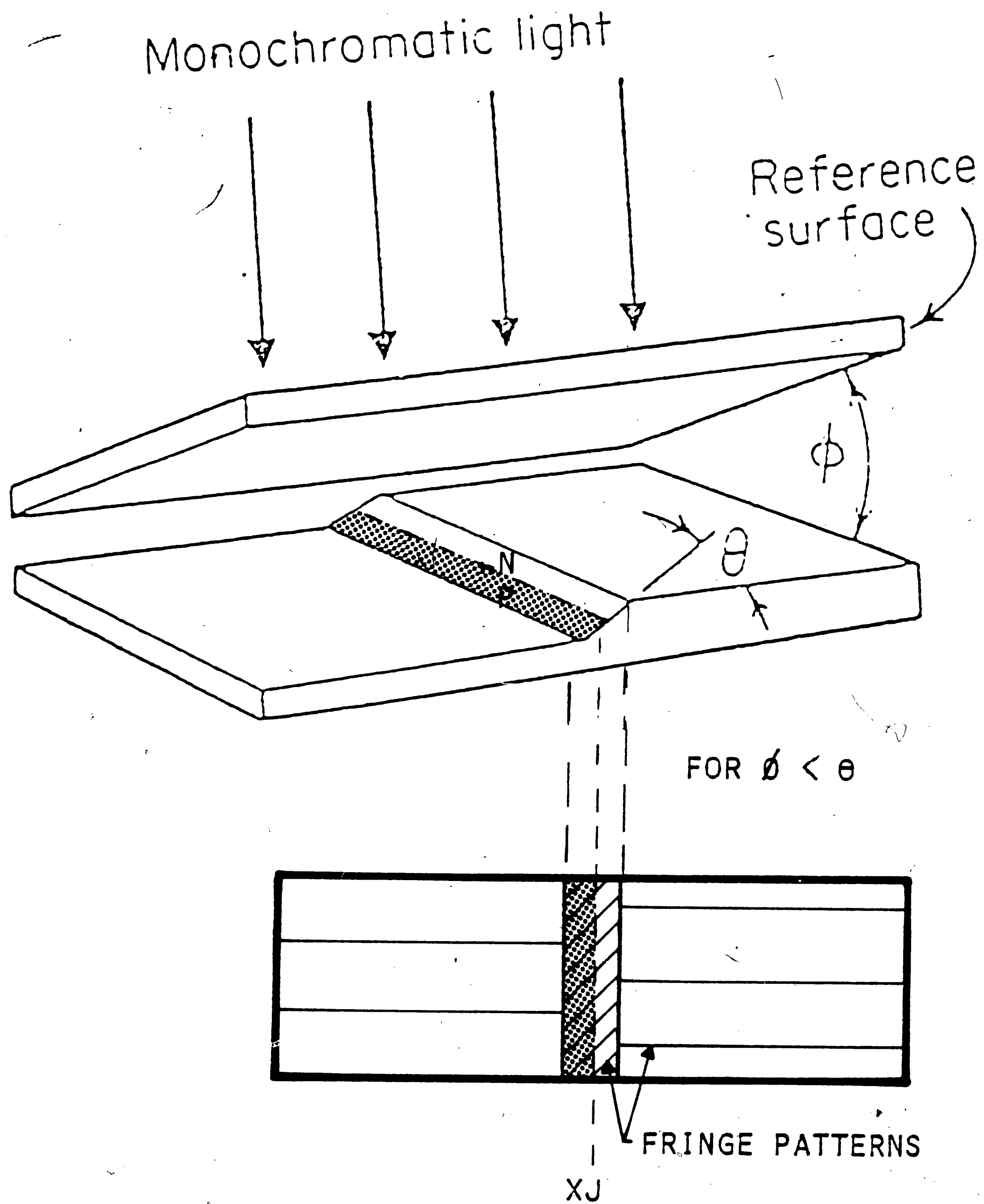
FIGURE 11

pressure which deforms the semiconductor surface directly underneath the probe tip. Also, the sample to be probed must be very smooth and flat since pits or scratches will produce noise and inaccuracies in the data.<sup>38</sup>

Besides the need for duplicating the measurement conditions, it is often necessary to apply theoretically derived correction factors to the raw spreading resistance data. Barrier effects, which may be extreme resistivity gradients in the sample ( $p^+n$  or  $n^+p$ ), distort the current flow pattern and can cause the observed spreading resistance values to vary up to a factor of ten when compared to the uniform, bulk sample of the same surface resistivity.<sup>33</sup> The effect of such boundaries is accounted for by calculating the appropriate "Dickey" correction factor for each point of the spreading profile.<sup>39</sup>

#### Angle-Lap and Staining

This technique determines the metallurgical junction depths of a transistor. The sample is bevelled and stained by a chemical solution of hydrofluoric acid plus 0.5 percent by volume nitric acid. Due to preferential oxidation of p-type silicon, the p-type areas stain dark.<sup>43</sup> Using a sodium vapor monochromatic light source ( $\lambda = 5890 \text{ \AA}$ ) and a partially reflecting reference plane extending out over the incline from the original surface, interference fringe patterns between the reference and the bevelled surface are produced. By counting the number of spaces between fringes, the junction depths can be determined (see Figure 12). Although this technique is easy to measure, the inaccuracy in determining the transition region between stained and non-stained silicon limits this technique to a relative comparison and not an exact measurement.<sup>37,40</sup>



DETERMINATION OF JUNCTION DEPTH  $X_J$  USING ANGLE-LAP AND STAIN MEASUREMENTS.

FIGURE 12

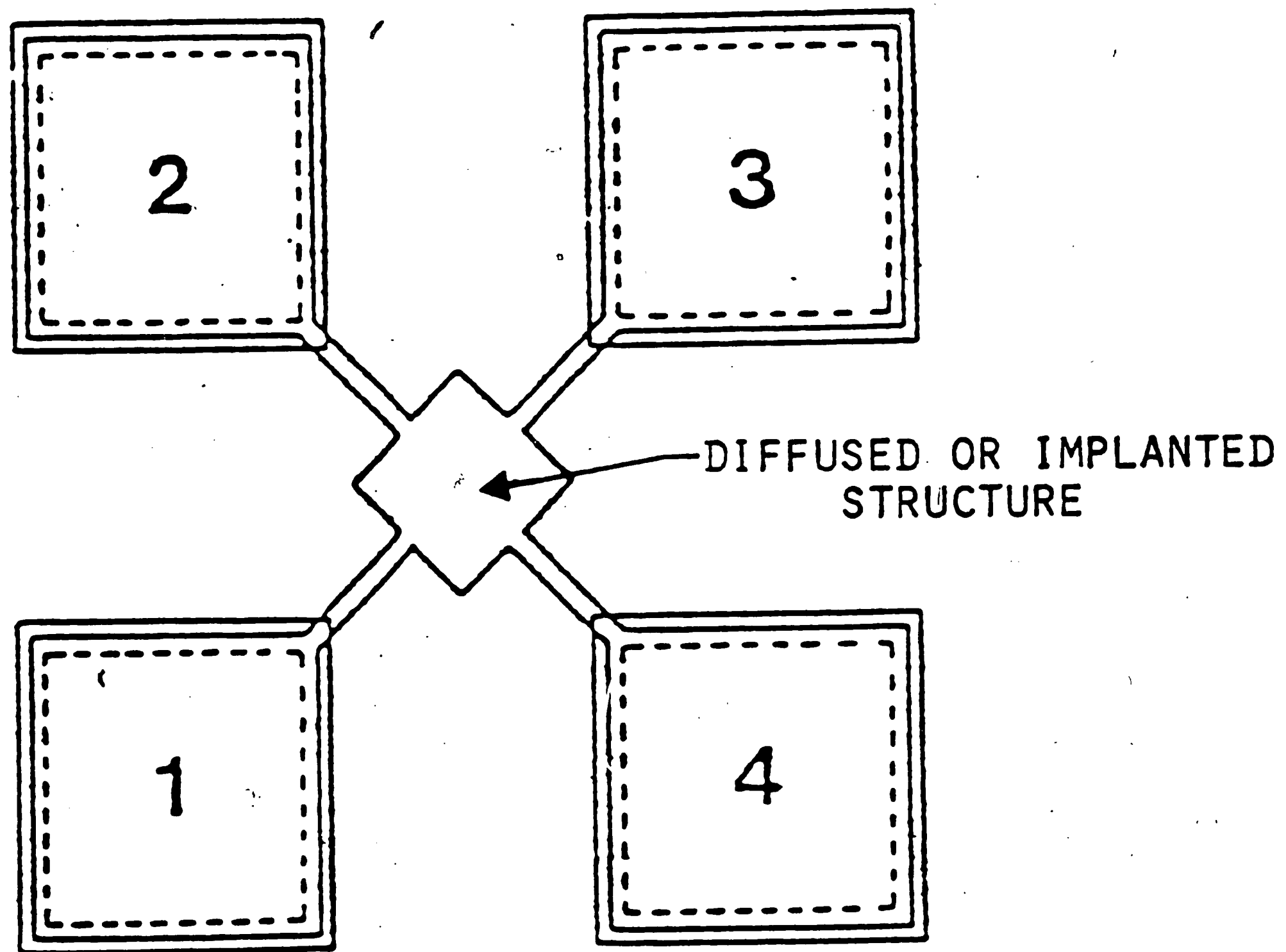
### van der Pauw (VDP) Sheet Resistance

This technique determines the sheet resistance (ohms/square) of diffused or implanted structures. In van der Pauw measurements, the voltage and current measurement terminals are cyclically connected to the probe pads and any two successive configurations are averaged to obtain a measurement. For a nominally symmetric van der Pauw structure (see Figure 13), the sheet resistance  $R_s$  is given by<sup>41</sup>

$$R_s = \pi (R_a + R_c) / (2 \ln 2) \quad (54)$$

where  $R_a = V_{23}/I_{14}$  and  $R_c = V_{34}/I_{12}$ . Ideally, these measurements are made with zero bias across the junctions. By multiplying the value of sheet resistance times the depth of the diffused or implanted layer, an average resistivity can be found. Once the resistivity is known, the average concentration can be determined by using Irvin's curves.





A VAN DER PAUW SHEET RESISTOR SUITABLE FOR CHARACTERIZING IMPURITY LAYERS. THE OUTER FOUR PADS ARE USED FOR PROBING THE STRUCTURE.

FIGURE 13

#### IV. EXPERIMENTAL RESULTS

The spreading resistance profiles (SRP) and SUPREM process simulations for the CBIC npn and pnp transistors are shown in Figures 14 and 15. The SUPREM process simulation profile is actually a similar program known as BICEPS developed by AT&T Bell Laboratories. A summary of the junction depths and zero-bias depletion region depths and electrical base widths obtained from numerically solving Poisson's equation (2) is shown in Table II below, using as input data the profiles determined by experiment (SRP) and process simulation (SUPREM).

TABLE II

$V_{CE} = 0$  volts

	Junction Depths ( $\times 10^{-4}$ cm)		Depletion Region Depths ( $\times 10^{-4}$ cm)			Electrical Base Width ( $\times 10^{-4}$ cm)
	XJEB	XJCB	XE	0	XB	$W_B$
<b>nnp</b>						
angle-lap	2.0	3.2				
SRP	1.73	2.93	1.61	1.82	2.66	0.84
SUPREM	1.05	3.44	0.99	1.08	3.13	2.05
<b>ppp</b>						
angle-lap	1.9	2.8				
SRP	1.97	2.76	1.85	2.14	2.49	0.35
SUPREM	2.33	3.60	2.20	2.43	3.26	0.83

By numerically integrating the area under the emitter and base profiles the total charge  $Q_E$  and  $Q_B$  can be determined. If we define  $N_{Eavg}$  and  $N_{Bavg}$  to be the average concentrations in the emitter and base respectively, so that

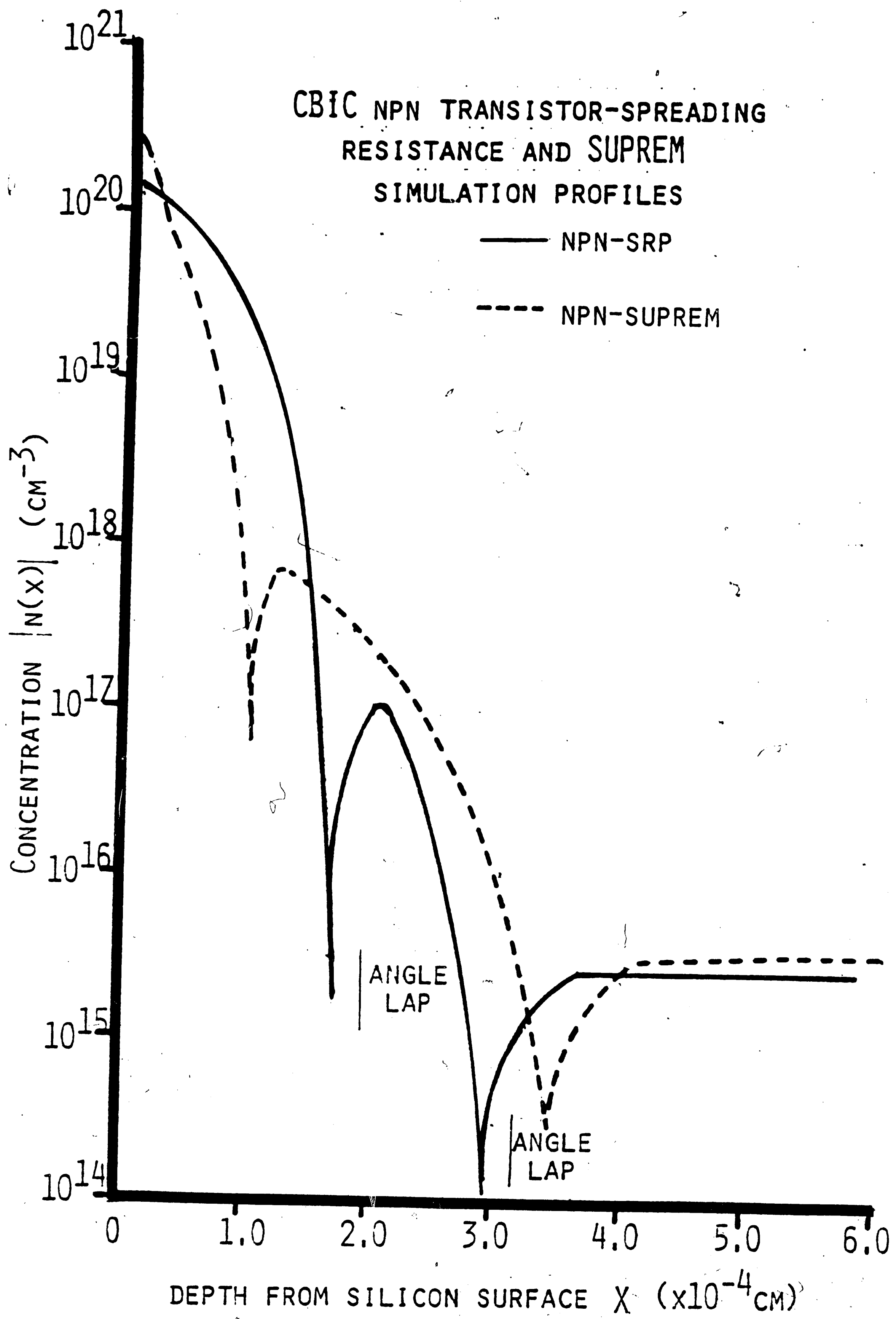


FIGURE 14

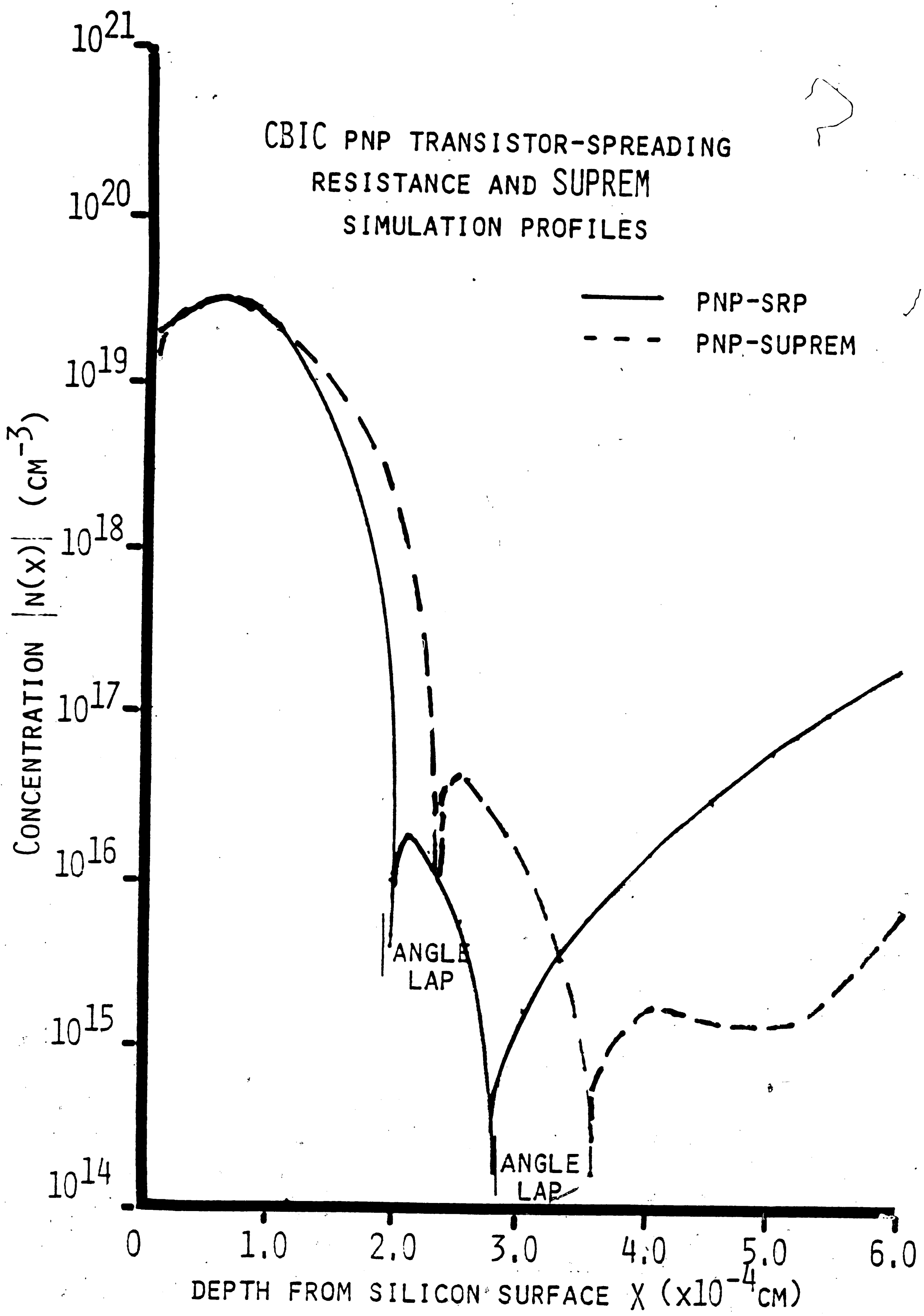


FIGURE 15

$$N_{Eavg} = Q_E/XE \quad (55)$$

and

$$N_{Bavg} = Q_B/W_B \quad (56)$$

the emitter sheet resistance  $R_{sE}$  and base-under-emitter sheet resistance  $R_{sBUE}$  can be evaluated from<sup>42</sup>

$$R_{sE} = 1/(q\mu Q_E) \quad (57)$$

and

$$R_{sBUE} = 1/(q\mu Q_B) \quad (58)$$

where  $\mu$  is the average majority carrier mobility calculated from equation (48).

A comparison of measured van der Pauw (VDP) sheet resistances and theoretically calculated sheet resistances from spreading resistance and SUPREM profiles is shown in Table III.

TABLE III

$V_{CE} = 0$  volts

	$Q_B$ ( $\times 10^{12} \text{ cm}^{-2}$ )	$N_{Bavg}$ ( $\times 10^{16} \text{ cm}^{-3}$ )	$R_{sBUE}$ ohms/square	$Q_E$ ( $\times 10^{15} \text{ cm}^{-2}$ )	$N_{Eavg}$ ( $\times 10^{19} \text{ cm}^{-3}$ )	$R_{sE}$ ohms/square
<b>nnp</b>						
SRP	5.08	6.05	4471	7.9	4.9	8.09
SUPREM	48.37	23.60	1479	5.9	6.0	10.93
VDP			3850			6.25
<b>ppn</b>						
SRP	0.48	1.37	10703	4.19	2.26	28.2
SUPREM	2.00	2.40	2748	3.43	1.56	33.5
VDP			2990			28.1

### Comparison of SRP and SUPREM

#### npn

The SRP predicts values of  $R_{sE}$  and  $R_{sBUE}$  much closer to the VDP measurements than the SUPREM simulation; therefore, the SRP was used to compare the theoretical results and electrical measurements of  $V_A$  and  $\beta$ .

#### pnp

Unlike the npn, the SUPREM simulation predicts the measured values for both  $R_{sE}$  and  $R_{sBUE}$  very accurately, while the SRP predicts a value for  $R_{sBUE}$  much higher than the VDP measurement. Although the value obtained for  $R_{sE}$  from the SRP is close to the VDP reading, the calculated value of  $R_{sBUE}$  is approximately 3.5 times higher than the VDP reading since the Gummel number  $Q_B$  is only  $4.8 \times 10^{11} \text{ cm}^{-2}$ . If we plot the electrical base width  $W_B$  versus the collector-to-base voltage  $V_{CB}$  (see Figure 16) obtained by numerically solving Poisson's equation (2), the data from the SRP indicates punch-through of the base ( $W_B = 0 \text{ } \mu\text{m}$ ) at only 10 volts. This is not possible since the measured breakdown voltage of the collector-base junction is 47 volts.

Therefore, the SUPREM simulation was used to compare the theoretical results with electrical measurements of  $V_A$  and  $\beta$ .

### Theoretical calculations of $V_A$ , $\beta$ , and $I_S$

#### 1. $V_A$

An arbitrary value of  $V_{CB} = 8$  volts was used to theoretically calculate the Early voltage  $V_A$  from equation (26). To find  $\partial W_B / \partial V_{CB}$  at  $V_{CB} = 8$  volts, the derivative of the fourth-order polynomial fit (represented by the smooth lines in

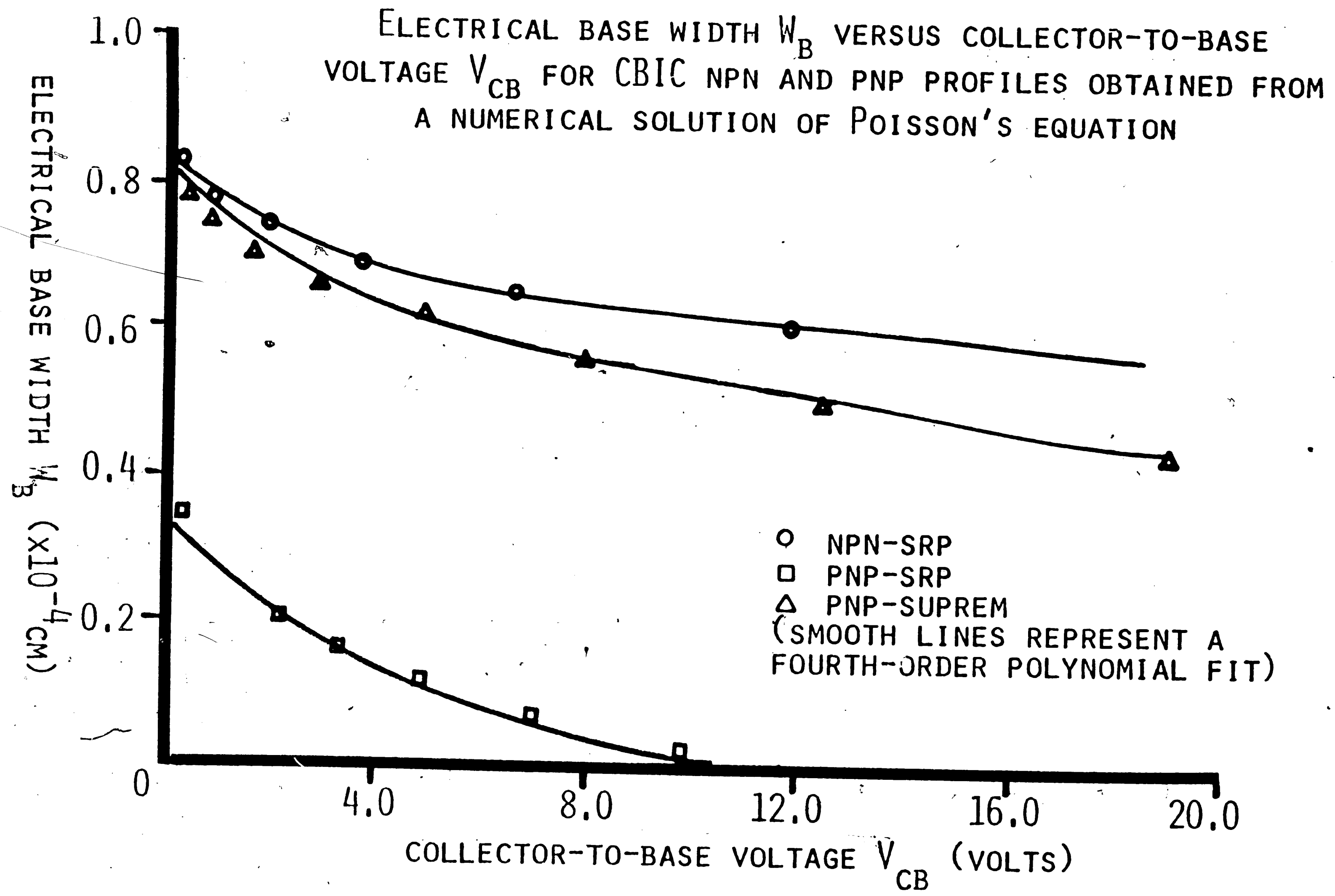


FIGURE 16

47

Figure 16) was evaluated.

## 2. $\beta$

To theoretically calculate the common-emitter current gain  $\beta$ , several parameters had to be determined. The minority carrier diffusion coefficients  $D_{mE}$  and  $D_{mB}$  were derived from the minority carrier mobilities using the Einstein relation. Both Muller and Kamins<sup>9</sup> equation (48) and Burk and De La Torre<sup>29</sup> equation (49) were evaluated as a way of comparing the difference in using majority carrier and minority carrier mobilities. The total bandgap narrowing  $\Delta E_g$  in the heavily doped emitter was determined by using equation (46) of Slotboom and De Graaff<sup>20</sup> for both n-type and p-type emitters. The effective emitter charge  $Q_{Eeff}$  was obtained from

$$Q_{Eeff} = Q_E \exp(-\Delta E_g/kT) \quad (59)$$

and it was used to compare calculated values of  $\beta$  from equation (37) with and without the bandgap narrowing phenomenon in the emitter. It was assumed that the base doping concentrations were low enough that bandgap narrowing in the base could be neglected.

## 3. $I_S$

The saturation current  $I_S$  was calculated from a straight forward evaluation of the equation shown below:

$$I_S = (q A_E D_{mB} n_i^2) / Q_B \quad (60)$$

Table IV shows the parameters used in the calculations of  $I_S$ ,  $V_A$ , and  $\beta$ . Table V compares the electrical measurements with theoretically calculated values of  $I_S$ ,  $V_A$ , and  $\beta$ .



TABLE IV

	<b>nnp</b> (SRP)	<b>npn</b> (SUPREM)
$A_E$ ( $\times 10^{-8}$ cm <sup>2</sup> )	400	324
$N_{Bavg}$ ( $\times 10^{16}$ cm <sup>-3</sup> )		
$V_{CB} = 0$ v	6.05	2.40
$V_{CB} = 2.5$ v	6.90	2.85
$V_{CB} = 8.0$ v	7.57	3.18
$D_{mB}$ (cm <sup>2</sup> /sec)		
$V_{CB} = 0$ v	23.8	8.89 (12.2)
$V_{CB} = 2.5$ v	23.0	8.55 (12.1)
$V_{CB} = 8.0$ v	22.3	8.34 (12.0)
$Q_B$ ( $\times 10^{12}$ cm <sup>-2</sup> )		
$V_{CB} = 0$ v	5.08	2.00
$V_{CB} = 2.5$ v	4.97	1.94
$V_{CB} = 8.0$ v	4.77	1.78
$N(XB)$ ( $\times 10^{16}$ cm <sup>-3</sup> )		
$V_{CB} = 8.0$ v	2.80	1.55
$\partial W_B / \partial V_{CB}$ ( $\times 10^{-6}$ cm/v)		
$V_{CB} = 8.0$ v	-0.81	-1.32
$N_{Eavg}$ ( $\times 10^{19}$ cm <sup>-3</sup> )	4.90	1.56
$D_{mE}$ (cm <sup>2</sup> /sec)	1.28 (.83)	2.74
$Q_E$ ( $\times 10^{15}$ cm <sup>-2</sup> )	7.90	3.43
$\Delta E_g$ (eV)	.120	.091
$Q_{Eeff}$ ( $\times 10^{13}$ cm <sup>-2</sup> )	6.89	9.41

The numbers in paranthesis ( ) are calculated using the minority carrier hole mobility equation (45) from Burk and De La Torre.<sup>29</sup>

TABLE V

	$I_s$ ( $\times 10^{-16}$ A)	$ V_A $ (volts)	$\beta$	
			no $\Delta E_g$	$\Delta E_g$
<b>nnp</b>				
electrical measurement	1.72	191.0		119
theory- SRP	2.99	210.3	28562	249 (384)
<b>ppn</b>				
electrical measurement	1.34	74.2		103
theory- SUPREM	2.30 (3.16)	87.0	5517	151 (214)

The numbers in paranthesis ( ) are calculated using the minority carrier hole mobility equation (45) from Burk and De La Torre.<sup>29</sup>

## V. DISCUSSION OF RESULTS

The emitter and base-under-emitter sheet resistances calculated from the spreading resistance profile of the npn agree quite well with the measured van der Pauw sheet resistances (see Table III). Although the emitter sheet resistance calculated from the spreading resistance profile of the pnp correlates well with the measured van der Pauw value, the base-under-emitter sheet resistance differs drastically from the van der Pauw reading. This large discrepancy in the value of  $R_{SBUE}$  for the pnp is apparently due to a very narrow electrical base width obtained from a numerical solution of Poisson's equation (see Table II, pnp-SRP,  $W_B = .35 \times 10^{-4}$  cm), and a low average base concentration in the n-type base (see Table III, pnp-SRP,  $N_{Bavg} = 1.37 \times 10^{16}$  cm<sup>-3</sup>). The Gummel number  $Q_B$ , numerically integrated under the base profile of the pnp, is only  $4.8 \times 10^{11}$  cm<sup>-2</sup>. The narrow electrical base width  $W_B$  and low Gummel number  $Q_B$  are unrealistic results since together they would predict a premature collector-base breakdown voltage of only 10 volts (see Figure 16). The low breakdown voltage of the collector-base junction, calculated from the spreading resistance profile of the pnp, is primarily due to the steep gradient of the collector profile at the collector-base junction (see Figure 15). The highly graded collector doping profile causes the collector-base depletion region to sweep into the base all the way to the emitter-base junction at only 10 volts. This low breakdown voltage is obviously not true since electrical measurements of  $I_C$  versus  $V_{CE}$  (see Figure 8) show the pnp transistor in the forward active region well beyond  $V_{CE} = 10$  volts.

From the data presented in Tables II and III we can conclude that the spreading

resistance profile of the pnp does not accurately represent the electrically active dopant profile in the pnp transistor, while the spreading resistance profile of the npn does represent fairly well the electrically active dopant profile in the npn transistor. The angle-lap and stain junction depth measurements, however, do agree with the metallurgical junction depths from both the npn and pnp spreading resistance profiles. But, the SUPREM simulation of the pnp, while predicting very accurately the measured values of sheet resistances, indicates the metallurgical junction depths of the emitter-base junction XJEB to be  $0.4 \mu\text{m}$  deeper and the collector-base junction XJCB to be  $0.8 \mu\text{m}$  deeper into the silicon surface (see Figure 15). A possible reason for this difference could be inaccuracies in the computer modelling of the high concentration  $p^+$  emitter profile and the impurity redistribution in the base after the  $p^+$  emitter implant-drive in. However, although the difference in junction depths between SUPREM and the spreading resistance of the pnp is significant, the difference in the shape and magnitude of the base and collector doping profiles is even more significant (especially when investigating the Early effect in bipolar transistors which depends highly on the Gummel number and the doping characteristics near the collector-base junction).

The fact that the npn spreading resistance profile accurately predicts electrical sheet resistance measurements while the pnp spreading resistance profile does not, is an unexpected result. There is a possibility that the extreme resistivity gradient, or barrier effect, associated with the emitter-base junction could distort the current flow pattern near the junction for a  $p^+n$  boundary causing the value of spreading resistance to appear much higher in the n base and the concentration derived

artificially lower. Also, if inaccuracies existed in the calibration curves and the theoretically derived correction factors for low p-type concentrations, the profile of the p collector could be significantly altered. But, regardless of the nature of the inaccuracy in the pnp SRP profile, there are two observations worthy of mention concerning the spreading resistance results in Figures 14 and 15: 1.) near the emitter-base junction, the peak concentration for the p base profile is reasonably accurate and the peak concentration for the n base profile of the pnp is low by perhaps a factor of three, and 2.) near the collector-base junction, the n collector profile of the npn is reasonably accurate and the p collector profile of the pnp is grossly distorted and highly suspect.

Besides base-under-emitter sheet resistance measurements, another indication of the accuracy of the profile in the base was determined by electrical measurements of the saturation current  $I_s$ . The value of  $I_s$  is inversely related to the Gummel number  $Q_B$  (see equation (60)). From Table V, we can see that the npn spreading resistance profile and the pnp SUPREM profile predicted values of  $I_s$  reasonably close to the actual measurements. This correlation lended support to the accuracy of the npn spreading resistance profile and the pnp SUPREM profile for characterizing the actual CBIC transistor electrical behavior.

The data presented in Table V indicates a very interesting result concerning the relationship between Early voltage  $V_A$  and common-emitter current gain  $\beta$ . Although the electrical measurement of current gain  $\beta$  is similar for both the npn and pnp transistors, the Early voltage  $V_A$  is significantly different. By examining the differences in the doping profiles of the npn and pnp transistors and theoretically

calculating values for  $V_A$  and  $\beta$ , the electrical measurements are shown to be predicted reasonably well.

If we compare the npn spreading resistance profile (Figure 14) with the pnp SUPREM profile (Figure 15), we can make several observations from  $0 < x < 6\mu\text{m}$ :

1. Emitter region

- a. **npn** - the  $n^+$  phosphorus emitter has a peak concentration slightly higher than  $10^{20} \text{ cm}^{-3}$  at the surface and the profile appears to follow a gaussian distribution to the emitter-base junction.
- b. **pnP** - the  $p^+$  boron emitter has a peak concentration much lower than the npn (only  $3 \times 10^{19} \text{ cm}^{-3}$ ) and it occurs  $0.5 \mu\text{m}$  deep into the silicon surface. The profile follows a steeper gradient to the emitter-base junction than the npn. This profile seems reasonable since the mass segregation coefficient of boron during thermal oxidation causes the boron to deplete from the silicon and accumulate in the  $\text{SiO}_2$  layer.

2. Base region

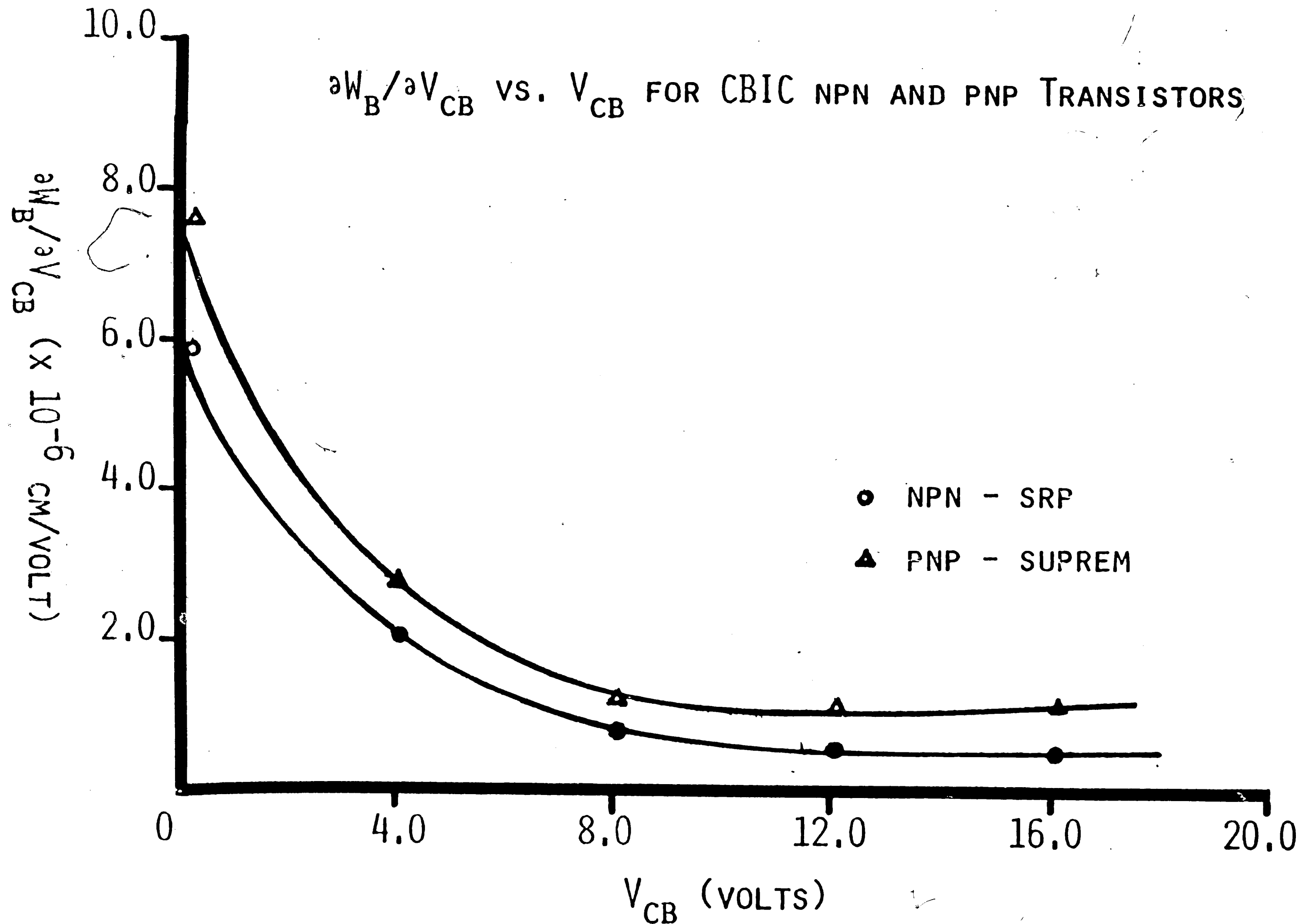
- a. **npn** - the boron base has a peak concentration of  $10^{17} \text{ cm}^{-3}$  and the profile follows a steep gradient to the collector-base junction. The steep gradient is expected since the boron is diffusing into a constant background concentration of the n-type epitaxial layer.
- b. **pnP** - the phosphorus base has a peak concentration of only  $3 \times 10^{16} \text{ cm}^{-3}$  and the profile follows a more gradual slope to the collector-base junction. The gradual slope is expected since the phosphorus is diffusing into a non-constant background concentration of the p-type

collector ( a  $p^+$  surface tub diffusing down and crossing a  $p^+$  buried layer diffusing up).

### 3. Collector Region

- a. **nnp** - the arsenic collector is a constant concentration epitaxial layer equal to  $2 \times 10^{15} \text{ cm}^{-3}$ .
- b. **pnp** - the boron collector profile is relatively flat for  $3.6 \mu\text{m} < x < 5.0 \mu\text{m}$  at  $2 \times 10^{15} \text{ cm}^{-3}$ , but it starts to increase sharply at  $5 \mu\text{m}$  due to the  $p^+$  buried layer up-diffusion.

The Early voltage  $V_A$ , as expressed in equation (26), is directly related to the characteristics of the doping profiles in the base and collector regions. Since the average concentration in the base is approximately three times higher for the nnp than the pnp and the electrical base widths are nearly identical, the Gummel number in the base should be higher for the nnp than the pnp. Also, since the base profile in the nnp is steeper than the pnp, and the n collector is constant unlike the p collector which increases sharply  $1.5 \mu\text{m}$  from the collector-base junction, the spread of the collector-base depletion region in the base, as a function of collector-to-base reverse bias  $V_{CB}$ , should be greater for the pnp than the nnp. The increase in the depletion layer width from the reversed biased collector-base junction corresponds to a decrease in the electrical base width  $W_B$ , and, therefore, we would expect  $\partial W_B / \partial V_{CB}$  to be higher for the pnp than the nnp. The data in Table IV supports the theoretical basis for the difference in  $Q_B$  and  $\partial W_B / \partial V_{CB}$  and Table V shows good agreement between theory and experimental results for  $V_A$ . If we plot  $\partial W_B / \partial V_{CB}$  versus  $V_{CB}$  (see Figure 17), we can see that for a given  $V_{CB}$ ,



$V_{CB}$  (VOLTS)

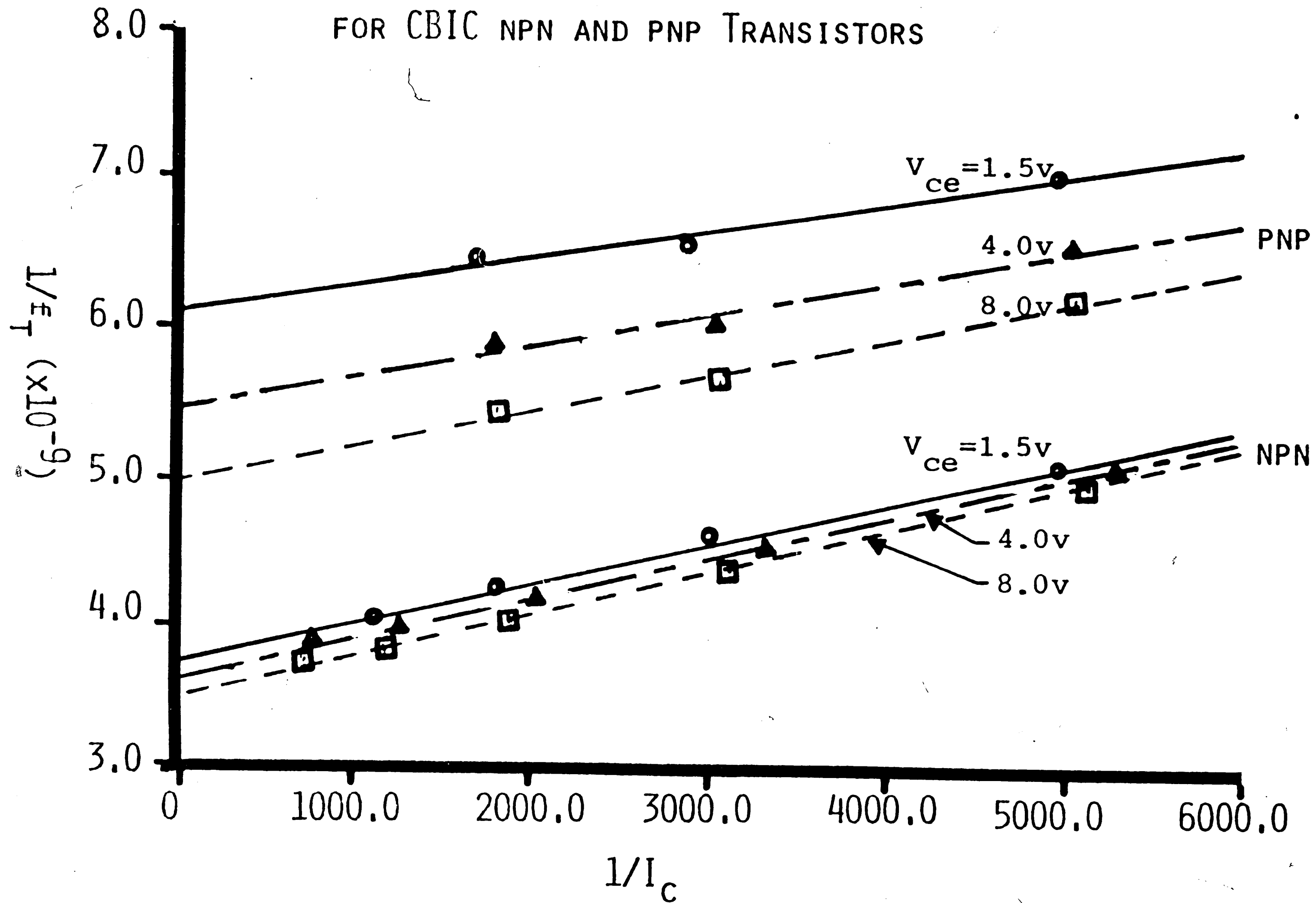
FIGURE 17



$\partial W_B / \partial V_{CB}$  is higher, as expected, for the pnp than the npn. Also, since the base transit time  $\tau_F$  is proportional to  $W_B^2$ , we would expect the  $\tau_F$  of the pnp to be a strong function of  $V_{CE}$  and to be a weak function for the npn. Figure 18 shows results of electrical measurements of the transition frequency  $f_T$  plotted as  $1/f_T$  versus  $1/I_C$ , where  $\tau_F$  is defined as  $1/2\pi f_T$  at  $1/I_C = 0$ . The data indicates, as expected, that as  $V_{CE}$  increases ( $V_{CB}$  increases),  $\tau_F$  increases significantly for the pnp, but it remains relatively unchanged for the npn.

The common-emitter current gain  $\beta$ , as expressed in equation (37), is directly related to the emitter and base doping profiles. Table V shows the large discrepancy between values of  $\beta$  calculated with and without bandgap narrowing effects in the emitter. If bandgap narrowing is not included in the theoretical calculations, the resulting value of  $\beta$  is several orders of magnitude higher than the measured value of  $\beta$ . The  $\beta$  calculated with bandgap narrowing, while not precisely accurate (high by a factor of 1.5 to 2.5 from the measured  $\beta$ ), is much closer than the  $\beta$  calculated without bandgap narrowing. There are several possibilities for the  $\beta$  calculated with bandgap narrowing being still slightly higher than the measured  $\beta$ . First, not all of the factors which tend to reduce the emitter efficiency, and, consequently,  $\beta$  have been quantitatively taken into account. Besides a reduction in the bandgap, the built-in electric field in the emitter is changing and at some distance into the emitter from the emitter-base junction, it aids the flow of minority carriers from the base to the emitter. Also, the probability of collisions between carriers is substantially increased in heavily doped silicon, and, therefore, Auger recombination increases which decreases the minority carrier lifetime. Second, since the effective emitter

ELECTRICAL MEASUREMENTS OF  $1/\epsilon_T$  VERSUS  $1/I_C$   
FOR CBIC NPN AND PNP TRANSISTORS



$1/I_C$   
FIGURE 18

charge  $Q_{Eeff}$  is exponentially dependent on  $\Delta E_g$  (see equation (59)), a small change in the value for  $\Delta E_g$  will modify  $Q_{Eeff}$  and, consequently,  $\beta$  significantly. Third, if we used the theoretical predictions of Bennett<sup>31</sup> which suggest that the minority carrier hole and electron mobilities are greater for doping concentrations exceeding  $2 \times 10^{19} \text{ cm}^{-3}$ , the minority carrier diffusion coefficients in the emitter would be greater and the theoretical values for  $\beta$  even closer to the electrical measurements.

Another important result in Table V is that the minority carrier hole mobilities from Burk and De La Torre<sup>29</sup> indicate a larger discrepancy in values for  $I_s$  and  $\beta$  than those calculated using Muller and Kamins.<sup>9</sup> However, it is obvious that the effects of bandgap narrowing in a heavily doped emitter must decrease the emitter efficiency in order to account for the measured electrical results.

## VI. CONCLUSION

The complementary npn and pnp bipolar transistors exhibit nearly identical common-emitter current gains, but the corresponding Early voltages are significantly different. The measured Early voltage of the npn transistor is almost three times higher than the pnp transistor (npn  $V_A = 191$  v, pnp  $V_A = 74.2$  v), even though the measured common-emitter current gains are approximately equal (npn  $\beta = 119$ , pnp  $\beta = 103$ ). This study provided a theoretical basis for the Early voltage difference.

In this study, no assumptions were made concerning the electrically active dopant profiles in the emitter, base, and collector regions. Spreading resistance measurements and a SUPREM simulation for a typical CBIC process were used to obtain the doping profiles for the npn and pnp transistors. Also, the depletion region widths of the emitter-base and collector-base junctions arising from the built-in potentials of the junction were included when determining the electrical base widths. A numerical solution of Poisson's equation was used to calculate the zero-bias depletion region widths and to obtain a fourth-order polynomial fit of  $W_B = f(V_{CB})$ .

The theory of the Early effect indicates that the Early voltage is strongly dependent on the Gummel number  $Q_B$  in the base and the narrowing of the electrical base width  $W_B$  as a function of collector-to-base reverse bias  $V_{CB}$ ,  $\partial W_B / \partial V_{CB}$ . By using the theoretically derived Early voltage expression (see equation (26)), we can predict the electrical measurements for CBIC npn and pnp transistors quite well (npn  $V_A$  calculated = 210.3 v, pnp  $V_A$  calculated = 87.0 v).

The difference in the npn and pnp Early voltages is due to the difference in the

base and collector doping profiles. The npn transistor has an average base doping concentration  $N_{Bavg}$  of  $6.05 \times 10^{16} \text{ cm}^{-3}$ , while the pnp transistor has an  $N_{Bavg}$  of only  $2.4 \times 10^{16} \text{ cm}^{-3}$ . The corresponding Gummel number is much higher for the npn ( $Q_B = 5.08 \times 10^{12} \text{ cm}^{-2}$ ) than the pnp ( $Q_B = 2.00 \times 10^{12} \text{ cm}^{-2}$ ). The gradient of the base profile towards the collector-base junction is much steeper for the npn than the pnp since the background concentration, into which the base dopant is diffused, is constant (n-type epitaxial layer) for the npn and graded for the pnp ( $p^+$  surface tub diffusing down and crossing a  $p^+$  buried layer diffusing up to form a self-isolated p-type collector region). Also, the collector profile for the npn is flat from the collector-base junction XJCB to  $x = 6 \times 10^{-4} \text{ cm}$ , while the pnp collector profile is relatively flat only from XJCB to  $x = 5 \times 10^{-4} \text{ cm}$  where it begins to increase substantially due to the  $p^+$  buried layer up-diffusion. As a result, the electrical base width decreases much faster for a given collector-to-base voltage, and, thus,  $\partial W_B / \partial V_{CB}$  is much higher for the pnp than the npn. Therefore, the higher  $Q_B$  and lower  $\partial W_B / \partial V_{CB}$  result in the Early voltage being higher for the npn than the pnp.

The common-emitter current gain  $\beta$  of modern planar transistors is emitter efficiency limited. Unless bandgap narrowing,  $\Delta E_g$ , effects in the heavily doped emitter are taken into account, the  $\beta$  calculated will be higher than the measured  $\beta$  by as much as two orders of magnitude. The effect of bandgap narrowing is to introduce an effective intrinsic carrier concentration  $n_{ie}$  which is exponentially dependent on  $\Delta E_g(N_{Eavg})$  and greater than the temperature dependent  $n_i$ . The emitter charge  $Q_E$  contributing to the injection of minority carriers into the base is,

therefore, reduced lowering the calculated  $\beta$  to a more realistic value. Using the experimental results of  $\Delta E_g$  presented by Slotboom and De Graaff<sup>20</sup> and the majority mobility expressions of Muller and Kamins<sup>9</sup>, the calculated values of  $\beta$  are only 1.5 to 2.5 times higher than measured. However, additional effects, which would tend to degrade the emitter efficiency, were not included in the calculation of  $\beta$ , and they are: 1.) since the effective emitter profile is lower than the actual emitter profile, the electric field at some location in the emitter may be in the opposite direction than expected and actually aid the minority carrier current flow from the base to the emitter, and 2.) as the carrier concentration increases, Auger recombination becomes dominant causing a reduction in the emitter minority carrier lifetime, which, in turn, reduces the emitter diffusion length. The calculated values of  $\beta$  can be reduced even further to more closely approximate the measured values according to Bennett's<sup>31</sup> theory which suggests that the minority carriers have higher mobilities than the majority carriers ( minority electron mobility/ majority electron mobility equals  $\cong 1.2$ , minority hole mobility/ majority hole mobility equals  $\cong 3$ ) at concentrations higher than  $2 \times 10^{19} \text{ cm}^{-3}$ . Using the higher minority hole mobilities measured by Burk and De La Torre<sup>29</sup> for  $10^{17} \text{ cm}^{-3} < N(x) < 10^{19} \text{ cm}^{-3}$ , however, the calculated values of  $\beta$  are even higher ( 2 to 4 times higher than measured) than those predicted using Muller and Kamins expression.

An interesting result of this study revealed the inaccuracy in using spreading resistance profiling to obtain the electrically active dopant profile in vertical pnp transistors. The base-under-emitter sheet resistance  $R_{sBUE}$  calculated from the pnp spreading resistance profile was four times higher than the van der Pauw reading,

while the  $R_{sBUE}$  of the npn spreading resistance profile showed good agreement with the van der Pauw reading. Also, the spreading resistance profiles of the n base and the p collector indicated a collector-base junction breakdown of only 10 volts which was impossible since the measured  $BV_{CB0}$  was 47 volts. The SUPREM simulation of the pnp provided a doping profile which accurately predicted the electrical behavior of the pnp transistor: however, the npn SUPREM simulation predicted values of emitter and base-under-emitter sheet resistances drastically different than the van der Pauw measurements.

In conclusion, the electrical results of the Early voltage and common-emitter current gain for complementary npn and pnp transistors can be theoretically explained both quantitatively and qualitatively. Using a SUPREM simulation, the  $V_A - \beta$  relationship could be optimized for improving the performance of the CBIC pnp transistor.



## REFERENCES

1. Early, J.M. "Effects of Space-Charge Widening in Junction Transistors" Proceedings of the I.R.E., Vol. 40 (1952), pp. 1401-1402.
2. Ebers, J.J., and Moll, J.L. "Large - Signal Behavior of Junction Transistors" Proceedings of the I.R.E., Vol. 42 (1954), pp. 1761-1772.
3. Lindholm, F.A., and Hamilton, D.J. "Incorporation of the Early Effect in the Ebers - Moll Model" Proceedings of the I.E.E.E., Vol. 59 (1971), p. 1378.
4. Jaeger, R.C., and Brodersen, A.J. "Self Consistent Bipolar Transistor Models for Computer Simulation" Solid-State Electronics, Vol. 21 (1978), pp.1269-1272.
5. Hart, B.L. "Offset Voltage, CMRR and PSRR of a Long - Tailed Pair: An Integrated Approach" Electronics Letters, Vol. 17 (1981), pp. 537-539.
6. Hart, B.L. "Incremental Output Resistance of a Wilson - Current Mirror" Proceedings of the I.E.E.E., Vol. 66 (1978), pp. 597-598.
7. Malone, F.D. "The Early Voltage of a Bipolar Transistor" I.E.E.E. Transactions on Electron Devices, Vol. 24 (1977), pp. 167-168.
8. Malhi, S.D.S., and Salama, C.A.T. "The Early Voltage of a Lateral PNP Transistor" Solid-State Electronics, Vol. 21 (1978), pp. 1187-1190.
9. Muller, R.S., and Kamins, T.I. Device Electronics for Integrated Circuits. New York : John Wiley & Sons, Inc., 1977.
10. Sze, S.M. Semiconductor Devices - Physics and Technology. New York : John Wiley & Sons, Inc., 1985.
11. Purcell, E.J. Calculus with Analytic Geometry - Third Edition. New Jersey : Prentice - Hall, Inc., 1978.
12. Gray, P.R., and Meyer, R.G. Analysis and Design of Analog Integrated Circuits - Second Edition. New York : John Wiley & Sons, Inc., 1984.
13. AT&T Bell Laboratories, Reading, Pennsylvania. Private communication with Kem K. Ferridun, Member of the Technical Staff, December, 1985.



14. Mertens, R.P., DeMan, H.J., and Van Overstraeten, R.J. "Calculation of the Emitter Efficiency of Bipolar Transistors" I.E.E.E. Transactions on Electron Devices, Vol. ed-20 (1973), pp.772-778.
15. DeMan, H.J. "The Influence of Heavy Doping on the Emitter Efficiency of a Bipolar Transistor" I.E.E.E. Transactions on Electron Devices, Vol. ed-18 (1971), pp.833-835.
16. Volfson, A.A., and Subashiev, V.K. "Fundamental Absorption Edge of Silicon Heavily Doped with Donor or Acceptor Impurities" Soviet Physics - Semiconductors, Vol. 1, no.3 (1967), pp.327-332.
17. Balkanski, M., Aziza, A., Amzallag, E. "Infrared Absorption in Heavily Doped n-Type Si" Physica Status Solidi, Vol. 31 (1969), pp.323-330.
18. Schmid, P.E. "Optical Absorption in Heavily Doped Silicon" Physics Review B., Vol. 23 (1981), pp.5531-5536.
19. Kleppinger, D.D., and Lindholm, F.A. "Impurity Concentration Dependent Density of States and Resulting Fermi Level for Silicon" Solid-State Electronics, Vol.14 (1971), pp.407-416.
20. Slotboom, J.W., and De Graaff, H.C. "Measurements of Bandgap Narrowing in Si Bipolar Transistors" Solid-State Electronics, Vol.19 (1976), pp.857-862.
21. Wieder, A.W. "Emitter Effects in Shallow Bipolar Devices: Measurements and Consequences" I.E.E.E. Transactions on Electron Devices, Vol. ed-27 (1980), pp.1492-1497.
22. Tang, D.D. "Heavy Doping Effects in p-n-p Bipolar Transistors" I.E.E.E. Transactions on Electron Devices, Vol. ed-27 (1980), pp.563-570.
23. Dhariwal, S.R., and Ojha, V.N. "Bandgap Narrowing in Heavily Doped Silicon" Solid-State Electronics, Vol.25 (1982), pp.909-911.
24. Stojadinovic, N.D., and Ristic, S.D. "Effects of Emitter Diffusion-Induced Stresses on the Common-Emitter Current Gain of Silicon Planar Transistors" Physica Status Solidi, Vol.(a) 51 (1979), pp.83-88.
25. Neugroschel, A., Pao, S.C., and Lindholm, F.A. "A Method for Determining Energy Gap Narrowing in Highly Doped Semiconductors" I.E.E.E Transactions on Electron Devices, Vol. ed-29 (1982), pp.894-902.
26. Lee, D.S., and Fossum, J.G. "Energy-Band Distortion in Highly Doped Silicon" I.E.E.E. Transactions on Electron Devices, Vol. ed-30 (1983), pp.626-634.

27. Del Alamo, J.A., and Swanson, R.M. "Comments on "A Method for Determining Energy Gap Narrowing in Highly Doped Semiconductors" I.E.E.E. Transactions on Electron Devices, Vol. ed-31 (1984), pp.123-124.
28. Dziwior, J., and Silber, D. "Minority-Carrier Diffusion Coefficients in Highly Doped Silicon" Applied Physics Letters, Vol. 35 (1979), pp.170-172.
29. Burk, D.E., and De La Torre, V. "An Empirical Fit to Minority Hole Mobilities" I.E.E.E. Electron Device Letters, Vol: edl-5 (1984), pp.231-233.
30. Fossum, J.G., Burk, D.E., and Yung, S.Y. "Effective Minority-Carrier Mobility in Heavily Doped Silicon Defined by Trapping and Energy-Gap Narrowing" I.E.E.E. Transactions on Electron Devices, Vol. ed-32 (1985), pp.1874-1877.
31. Bennett, H.S. "Hole and Electron Mobilities in Heavily Doped Silicon: Comparison of Theory and Experiment" Solid-State Electronics, Vol. 26 (1983), pp.1157-1166.
32. Bennett, H.S. "Improved Concepts for Predicting the Electrical Behavior of Bipolar Structures in Silicon" I.E.E.E. Transactions on Electron Devices, Vol. ed-30 (1983), pp.920-927.
33. Davis, P.C., and Moyer, S.F. "Ion Implanted, Compatible Complementary PNP's for High Slew Rate Operational Amplifiers" Paper presented at the International Electron Devices Meeting, Washington, D.C., December 4-6, 1972.
34. Davis, P.C., Moyer, S.F., and Saari, V.R. "High Slew Rate Monolithic Operational Amplifier Using Compatible Complementary PNP's" I.E.E.E. Journal of Solid-State Circuits, Vol. sc-9 (1974), pp.340-347.
35. Davis, P.C., Graczyk, J.F., Griffin, W.A. "Design of an Integrated Circuit for the T1C Low-Power Line Repeater" I.E.E.E. Journal of Solid-State Circuits, Vol. sc-14 (1979), pp.109-120.
36. Berglund, R.K. "Practical Approach to Monitoring of Implanted Layers" Semiconductor International - May 1984, pp.155-159.
37. Runyan, W.R. Semiconductor Measurements and Instrumentation. New York: McGraw-Hill Book Co., 1975.
38. Malkiel, C. "Spreading Resistance Profiling: A Technique for Measuring Dopant Concentrations" Test & Measurement World - January 1982, pp.63-65.

39. Dickey, D.H. "Two-Point Probe Correction Factors" NBS Special Publication 400-10 Spreading Resistance Symposium , 1974, pp.45-50.
40. AT&T Technology Systems, Reading, Pennsylvania. Private communication with Jim W. Brossman, Senior Engineer, February 1986.
41. Lafayette College, Easton, Pennsylvania. Private communication with Thomas A. Reilly, Associate Professor of Electrical Engineering, March 1986.
42. Sze, S.M. VLSI Technology. New York: McGraw-Hill Book Company, 1983.
43. Ghandhi, S.K. The Theory and Practice of Microelectronics. New York: John Wiley & Sons, Inc., 1968.
44. Colclaser, R.A. Microelectronics - Processing and Device Design. New York: John Wiley & Sons, Inc., 1980.

## VITA

The author was born on January 19, 1961, in Abington, Pennsylvania, and is the son of Mrs. Sylvia E. Parks and Mr. Richard E. Parks. In 1978, he graduated from Upper Moreland Senior High School in Willow Grove, Pennsylvania, and he enrolled at Lafayette College in Easton, Pennsylvania. As an undergraduate at Lafayette, he became a member of the Institute of Electrical and Electronic Engineers and Eta Kappa Nu. He graduated in 1982 with a Bachelor of Science degree in Electrical Engineering. After graduation, he pursued part-time graduate studies at Lehigh University in Bethlehem, Pennsylvania, and he worked full-time at AT&T Technology Systems in Reading, Pennsylvania as a product engineer in the Linear Bipolar Device Technology and Development Department. He is currently a bipolar integrated circuit design engineer at AT&T, and he will complete the requirements for the Master of Science degree in Electrical Engineering in 1986.